

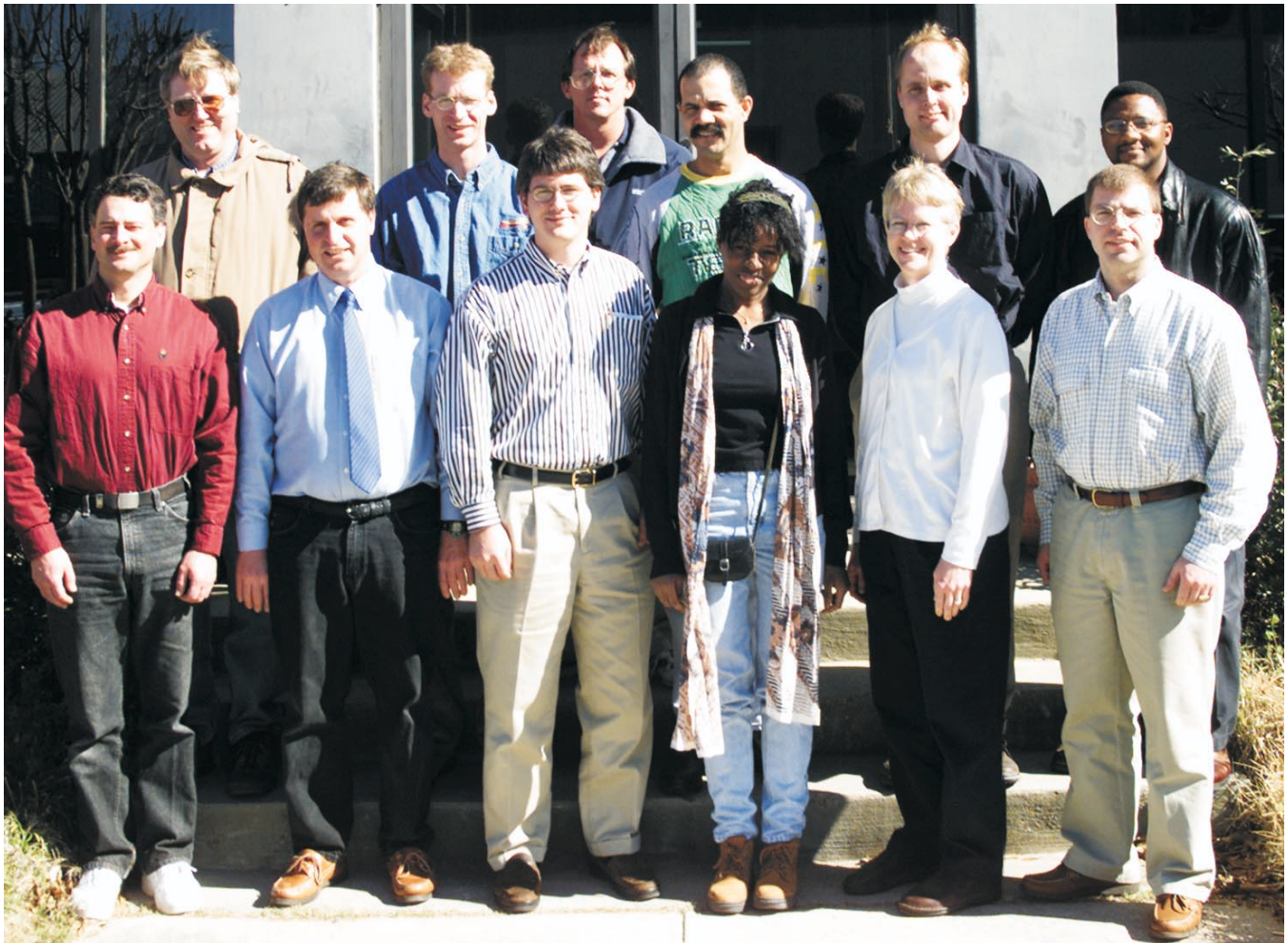
Coastal and Hydraulics News

Coastal and Hydraulics Laboratory
U.S. Army Engineer Research and Development Center
Vicksburg, Mississippi USA 39180-6199

Vol CHL-00-1

November 2000

Coastal Engineering Prospect Course Held in Vicksburg



Attendees of the FY2000 Coastal Engineering Prospect Course:

First row from left - Richard Gunsolus, Portand District; Rick Tuers, New York Department of Environmental Conservation; Eddie Wiggins, Mobile District; Odile Accilien, New York District; Tracy Lesser, Jacksonville District; and James Selegean, Detroit District.

Second row from left - Richard Powell, Jacksonville District; Lt. Pete Carroll, U.S. Coast Guard; Jim Fields, Los Angeles District; Burnell Thibodeaux, New Orleans District; Karl Ahlen, New York District; and Jonas White, Jacksonville District.

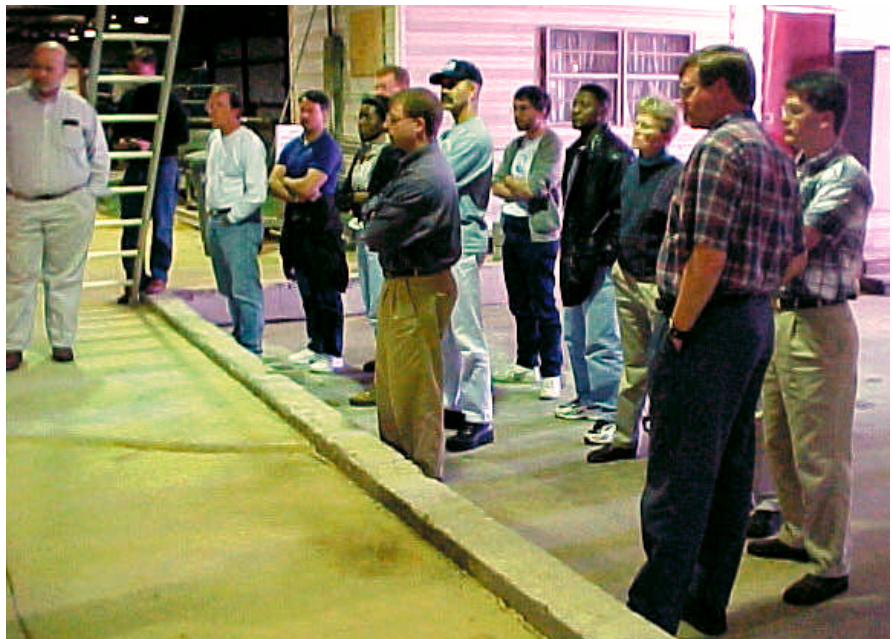
Introduction and Overview

A revised Coastal Engineering Prospect Course was conducted by the U.S. Army Engineer Research and Development Center (ERDC) at the Waterways Experiment Station in Vicksburg, MS, on February 1-10, 2000. This eight-day training course was developed around the new Coastal Engineering Manual (CEM), which is replacing the venerable Shore Protection Manual (SPM). The Coastal Engineering course was attended by 10 engineers from Corps District offices, a civil/ocean engineer from the U.S. Coast Guard, and an environmental engineer from the New York State Department of Environmental Conservation.

This new prospect course combined topics previously covered in two separate one-week courses. The expanded duration of the new Coastal Engineering course allowed a coordinated and comprehensive in-depth technical study of nearly all aspects of coastal engineering covered in the new CEM. The course was aimed at engineers involved in coastal engineering design, project construction, project management, and operations and maintenance. (A companion five-day course, "Coastal Project Planning," provides a less technical overview of coastal engineering issues for planners and managers who oversee coastal projects and must understand issues faced by coastal engineers.)

Course Topics

One key objective in developing the new Coastal Engineering prospect course was assuring a logical arrangement of related topics separated into half-day instruction modules. Many of the half-day modules are comprehensive enough to be presented as stand-alone sessions. A chronological listing of the course modules and the associated instruction topics is given in the table. The modularity of the instruction topics provides flexibility in presenting the prospect course in the future because some modules can be moved around in the schedule to



accommodate class needs and instructor availability.

Excursions and Tours

Classroom lectures and design exercises were complemented with excursions to the laboratory model facilities and to the ship simulator located at ERDC. At the ship simulator, principal investigator Dennis Webb explained the operation of the computer-driven simulator, then students were given an opportunity to steer (and sometimes run aground) a large bulk carrier as it entered a navigation channel.

The laboratory tour was led by Dennis Markle, and it featured stops at the Los Angeles/Long Beach Harbor model, the testing facility for the Rapidly Installed Breakwater System, the Barber's Point Harbor model, a flume study of breakwater stability, and the generic inlet model facility.

Technology Transfer Fair

Throughout the course, students were introduced to various computer-based tools developed by CHL and made available for Corps use. The "Technology Transfer Fair," an informal event held on the final morning of the short course, provided the students an opportunity to gain hands-on experience with most of the PC-based software demonstrated earlier in the course. Experts were on hand to instruct in program usage, to give guidance on program applicability for various problems, and to answer questions about how to obtain and install the programs. Students moved around the room to the various computers according to their interests and needs. In addition to learning more about available computer tools, they established contacts with the CHL engineers and scientists who are responsible for assuring the programs meet the needs of the field. This will promote a two-way information exchange between the program developers and the end-users which will be mutually beneficial.

Instruction Modules in Coastal Engineering Prospect Course	
Day 1: Overview of Coastal Hydrodynamics	<p>Morning Module: Introduction to Coastal Engineering and Water Waves Course Preliminaries, Pre-Test Introduction to Coastal Engineering Waves and Wave Theories</p> <p>Afternoon Module: Long Wave Processes Wave Prediction and Transformation for Engineering Design Water Levels and Long Waves Harbor Hydrodynamics Hydrodynamics for Design</p>
Day 2: Project Planning	<p>Morning Module: Elements of Project Planning Geological Setting and Diversities Overview of Sediment Transport Project Development Site Characterization</p> <p>Afternoon Module: Functional Design Issues Shore Protection Navigation Environmental/Restoration Navigation at Entrances (Ship Simulator Tour)</p>
Day 3: Design of Sloping-Front Structures	<p>Morning Module: Fundamentals of Design Structure Types and Failure Modes Wave Runup and Overtopping Wave Transmission and Reflection Rubble-Mound Structure Stability</p> <p>Afternoon Module: Sloping-Front Structure Risk Analysis and Construction Materials Concrete Armor Units Incorporating Risk into Design Construction Materials Composite Design Example</p>
Day 4: Design of Vertical-Front Structures	<p>Morning Module: Fundamentals of Design Wave Runup, Overtopping, Transmission, Reflection Toe Stability/Filter Layer Design Forces on Structures Caisson Stability</p> <p>Afternoon Module: Foundations, Scour, and Construction Materials Floating Structures (tour of RIBS laboratory facility) Coastal Structure Foundations Scour and Scour Protection Jet Scour at Inlets</p>
Day 5: Beach Fills and Shoreline Change	<p>Morning Module: Engineering Problems and Design of Beach Fills Sediment Transport Processes in the Coastal Zone Introduction to Beach Nourishment Design Design of Beach Fill Cross Section Beach Fill Planform Design Considerations</p> <p>Afternoon Module: Example Applications Construction and Monitoring of Beach Fills Sediment Budget Analysis Beach Fill Design Example Dune Design Example</p>
Day 6: Inlet Engineering	<p>Morning Module: Tools for Inlet Engineering Inlet Processes Inlets Online Sediment Budgets at Inlets Waves and Currents at Inlets</p> <p>Afternoon Module: Inlet Example Applications Field Measurements at Inlets Sediment Budget Example Tidal Circulation Example Inlet Geomorphology and Predictive Models</p>
Day 7: Project Maintenance and Review of Design Tools	<p>Morning Module: Dredging and Project Maintenance Dredging Fundamentals Coastal Aspects of Dredging Sand Bypassing Issues Monitoring and Rehabilitation</p> <p>Afternoon Module: Overview of Design Examples Physical Modeling Tour of Physical Model Areas Automated Coastal Engineering System Overview of Available Tools</p>
Day 8: Technology Transfer	<p>Morning: Technology Transfer Fair</p>

Summary

The 12 engineers in the FY2000 edition of the Coastal Engineering Prospect Course distinguished themselves by their enthusiasm, attentiveness, and practical engineering slant they brought to the prospect course. A tremendous amount of technical material was presented over the eight days of the Coastal Engineering course, and the students took home an equally large amount of engineering guidance that will serve them in their careers. The Corps Districts should be proud of the high quality of these young engineers who will become the future technical leaders in the field of coastal engineering.

Next offering of the Coastal Engineering Prospect Course

The Coastal Engineering Prospect Course is scheduled for presentation at two-year intervals with the next course being offered in winter of FY2002. For further information about this prospect course, contact Dr. Steven Hughes at e-mail address: HughesS@wes.army.mil. (See the adjacent box for details about specialized onsite CEM short courses.)

An additional benefit of modular course design used in the Coastal Engineering Prospect Course (and also in the Coastal Project Planning Course) is that CHL can easily develop and present customized short courses at District offices. Such a short course would consist of a subset of the modules listed in the table that are of specific interest to a particular District. For example, a District could design a two-day course that focuses on beach fills and shoreline change. In addition to Corps staff, the District might want to invite engineers from state and local jurisdictions and AE firms. This would be a cost-effective way to provide needed specialized training to those engineers who will most directly benefit.

For more information about onsite CEM-related short courses, contact Dr. Steven Hughes at e-mail address: HughesS@wes.army.mil.





Simulation of Flow in Hydraulic Structures Using ADH

Richard L. Stockstill¹ and R. C. Berger¹

Introduction

This paper describes a process of modeling flow in hydraulic structures. In particular, application is made with the unstructured flow solver, ADH (ADaptive Hydrology model). ADH also contains solvers for groundwater and two-dimensional shallow water flows. It is capable of refining or coarsening the grid based on error estimates during flow calculations. Modeling of hydraulic structures presents many computational challenges to design/evaluation engineers. Hydraulic structures often have components containing internal (pressure) flow while other components hold external (free-surface) flow. Therefore, three-dimensional (non-hydrostatic) codes must account for both regions of fixed domain limits and regions that have time-varying domains due to movement of the free surface. Multiple regions of rapid accelerations also characterize hydraulic structures as water passes from slow reservoir flow to high-velocity conduit flow. This difference translates to significant differences in Reynolds number over various portions of the modeled flow field. Free-surface applications to steep channels such as chutes require a model that produces stable solutions for a large range of Froude numbers. The model must solve subcritical and supercritical flow fields and resolve any transitions between these regimes. These flow fields may contain shocks such as oblique standing waves and hydraulic jumps. These solutions may include a highly contorted free surface, and thus requires a robust free-surface model. Finally, the geometric complexity of most hydraulic structures necessitates the use of CAD (Computer Aided Design/

Drafting) modeling which leads to a need for a CAD-to-grid generator interface. Visualization, of course, is also important for the engineer to examine the geometric design and the resulting hydraulic conditions.

Modeling Procedure

The process of developing computational models of hydraulic structures begins with a three-dimensional CAD description of the parameter-based geometry. This CAD information is then fed to a grid generator where the domain is discretized into a tetrahedral mesh required by ADH. The resulting mesh in conjunction with specified boundary conditions are then passed as input to the flow solver. The resulting solution must next be transferred to a visualization tool to facilitate the evaluation of the hydraulic conditions within the structure. The flow solver is capable of determining the internal pressure and elevation of the free surface in conjunction with the three velocity components without assuming hydrostatic pressure distribution. The ADH code is written to take advantage of the newest multiple-processor machines of the Major Shared Resource Center (MSRC).

Applications

Application of ADH has been made to hydraulic structures varying from high-velocity channels to navigation components. This paper presents three applications as demonstrations of the modeling process, and it documents the model's features and capabilities.

CAD-to-Grid Process Applied to an Intake

The first application is a model of the Marmet Navigation Lock intake structure. The multiported intake model demonstrates the required CAD-to-Grid process for complicated geometries. The intake modeled about 215 m of the upper approach, the upper miter gates and recesses, the intake ports, and filling system culverts as shown in the CAD drawing provided in Figure 1. The tetrahedral mesh, shown on Figure 2, had 20,194 nodes and 87,953 elements. Figure 3 shows the details of the discretization near the intake ports. Flow in the approach channel is slow and deep. The flow accelerates as it enters the intake ports. Further accelerations occur as the port flows combine into a single culvert on each half of the structure. These accelerations are shown in the velocity and pressure contours along a plane located in the center of the culvert beginning at the port faces (Figures 4 and 5, respectively).

Scalability Demonstrated with Outlet Manifold

Next, the parallel performance of the ADH code is shown by application of the flow model to a multiported navigation lock outlet. The outlet model is an application requiring high resolution to describe the port shapes as shown on the surface mesh of Figure 6. The tetrahedral mesh had 48,000 nodes and 244,000 elements. Initial runs were made to obtain computational timing information for documentation of ADH's scalability. The model was run on a Department of Defense (DoD) High-Performance Computing

¹ Research Hydraulic Engineer, U.S. Army Engineer Research and Development Center, Coastal and Hydraulics Laboratory, 3909 Halls Ferry Road, Vicksburg, MS 39180-6199.

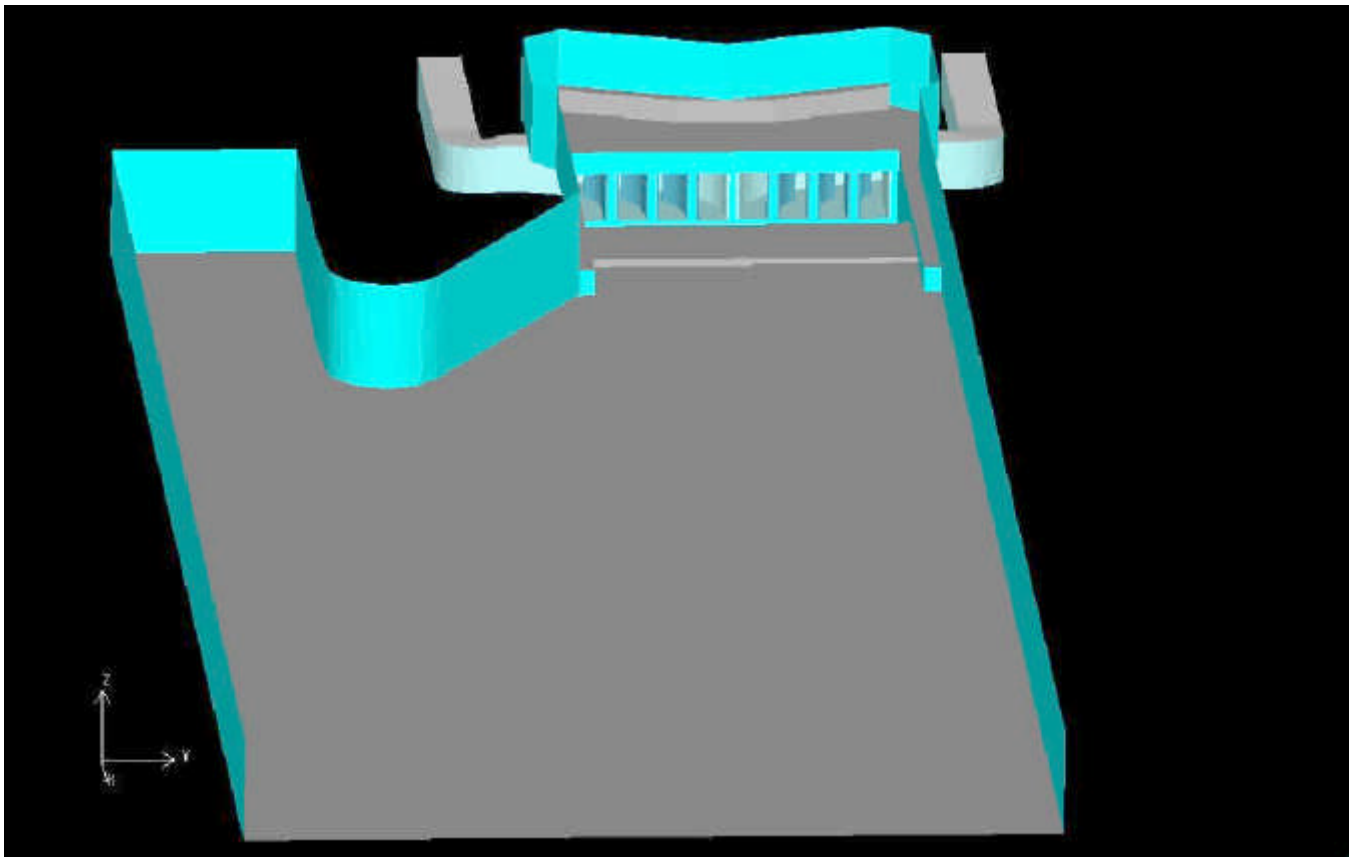


Figure 1. Three-dimensional CAD model of lock intake

Center's Cray T3E. The multiple processor speedups are illustrated by the timings presented in Figure 7. Significant speedups were obtained when up to 64 processors were used. Additional processors did not speed up the computation time in this application due to the larger relative communication time required between processors. This is a relatively small test case. Parallel performance will be even better for larger problems. The flow solution is shown on the velocity contours plotted on a horizontal plane through the center of the structure (Figure 8).

Free-Surface Capability Demonstrated with Supercritical Flow Contraction

Finally, free-surface capabilities are demonstrated by application to a

supercritical flow contraction having an approach Froude number of 4. This application demonstrates ADH's free-surface modeling capabilities in flow fields having multiple shocks. The free-surface solution is challenging due to the presence of oblique standing waves within and downstream of the transition. The flow solution is presented on the steady-state finite element mesh shown in Figure 9. The top of the mesh maps the oblique standing waves generated within the contraction.

Summary and Conclusions

The ADH flow solver will provide a rapid and economical method of predicting the hydrodynamic conditions in and around hydraulic structures. The parallel code allows

reasonable computational time requirements for extremely large problems.

Recommendations for Further Research

Accurate modeling of hydraulic structures requires accounting for turbulence effects. Shear stresses generated at fixed boundaries play an important role in the composition of flow in conduits and channels. Future efforts should include the development of a turbulence model within ADH.

Acknowledgments

Funding for this effort is provided by the DoD High Performance Computing Modernization Office through the Common High-Performance Software Support Initiative (CHSSI).

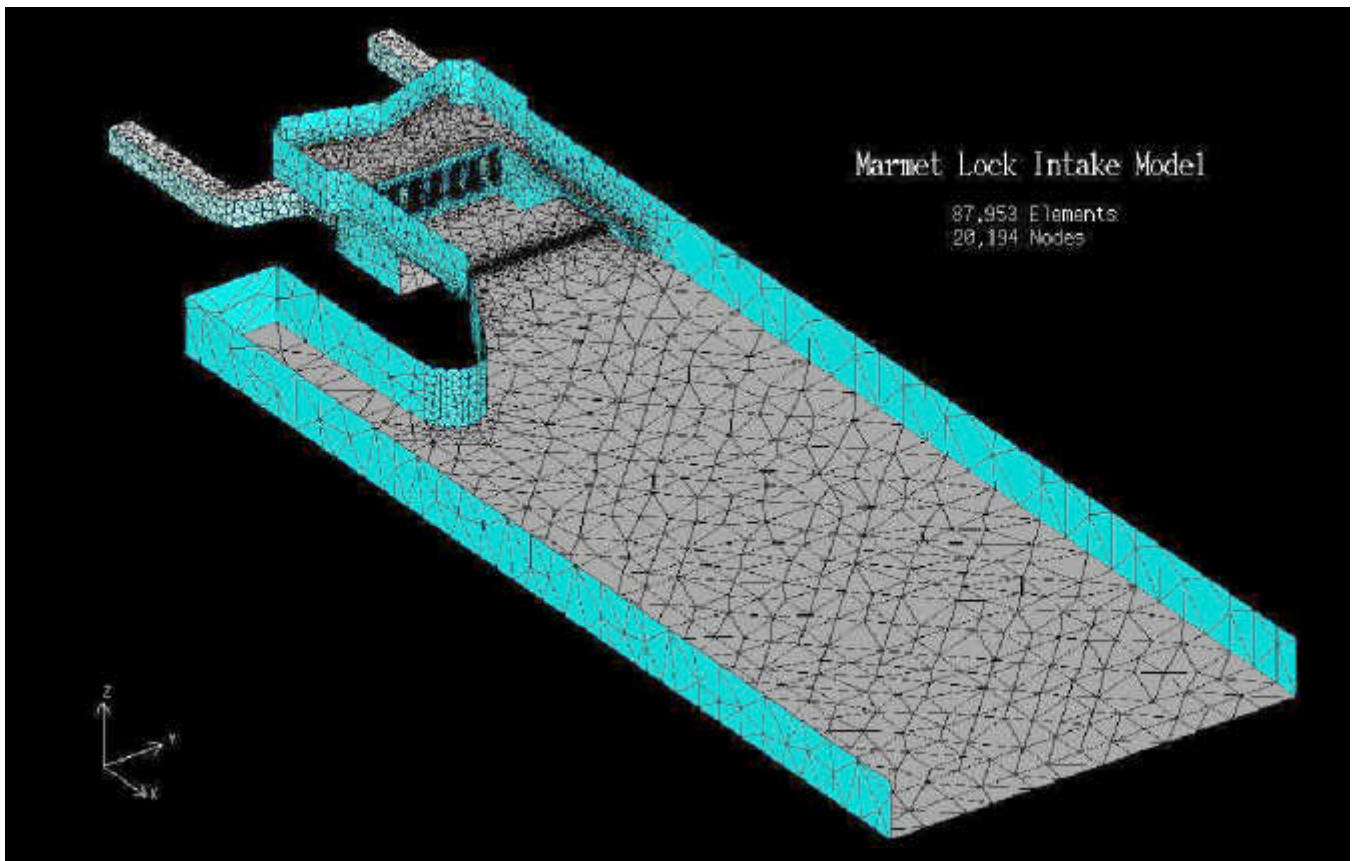


Figure 2. Surface mesh of lock intake

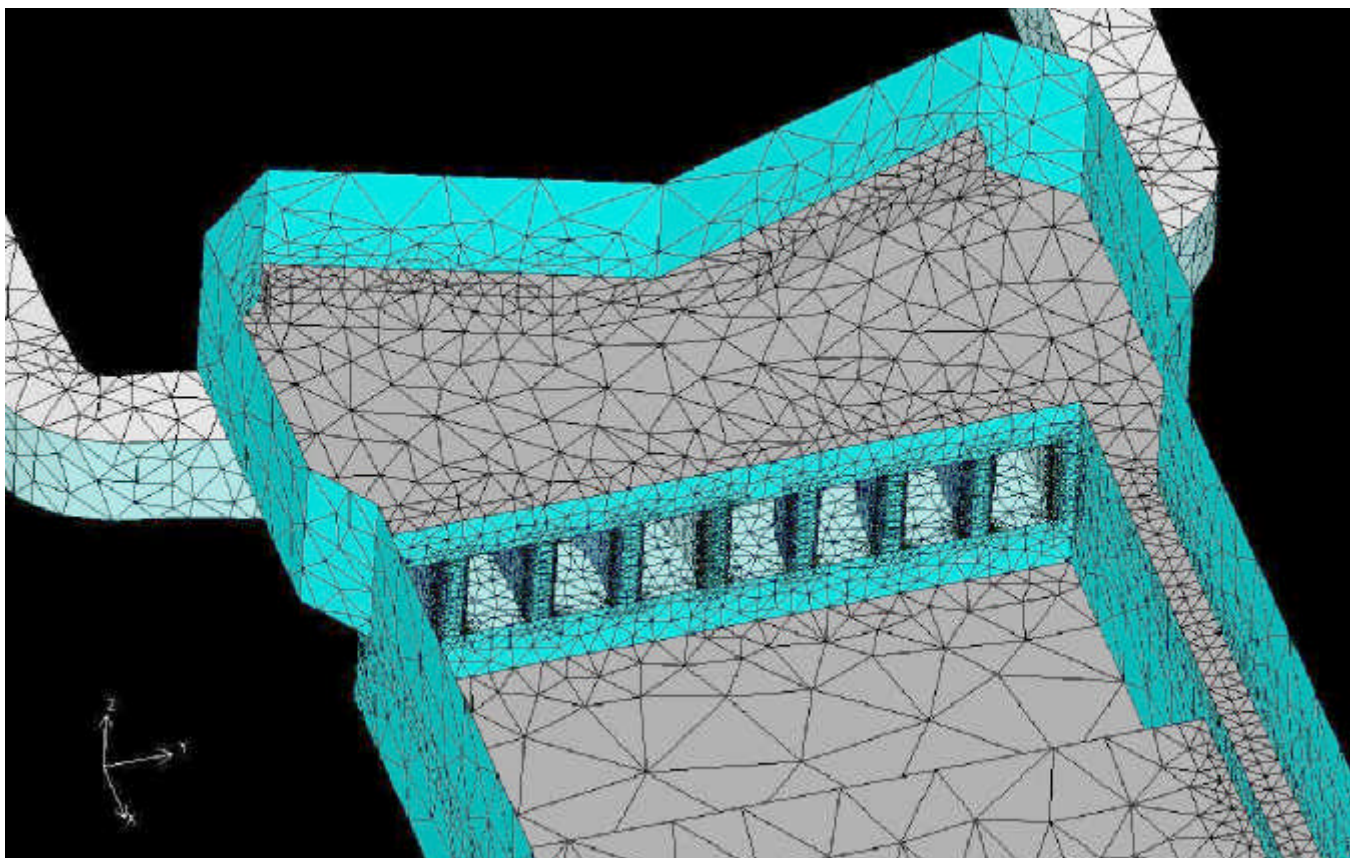


Figure 3. Surface model at the port faces

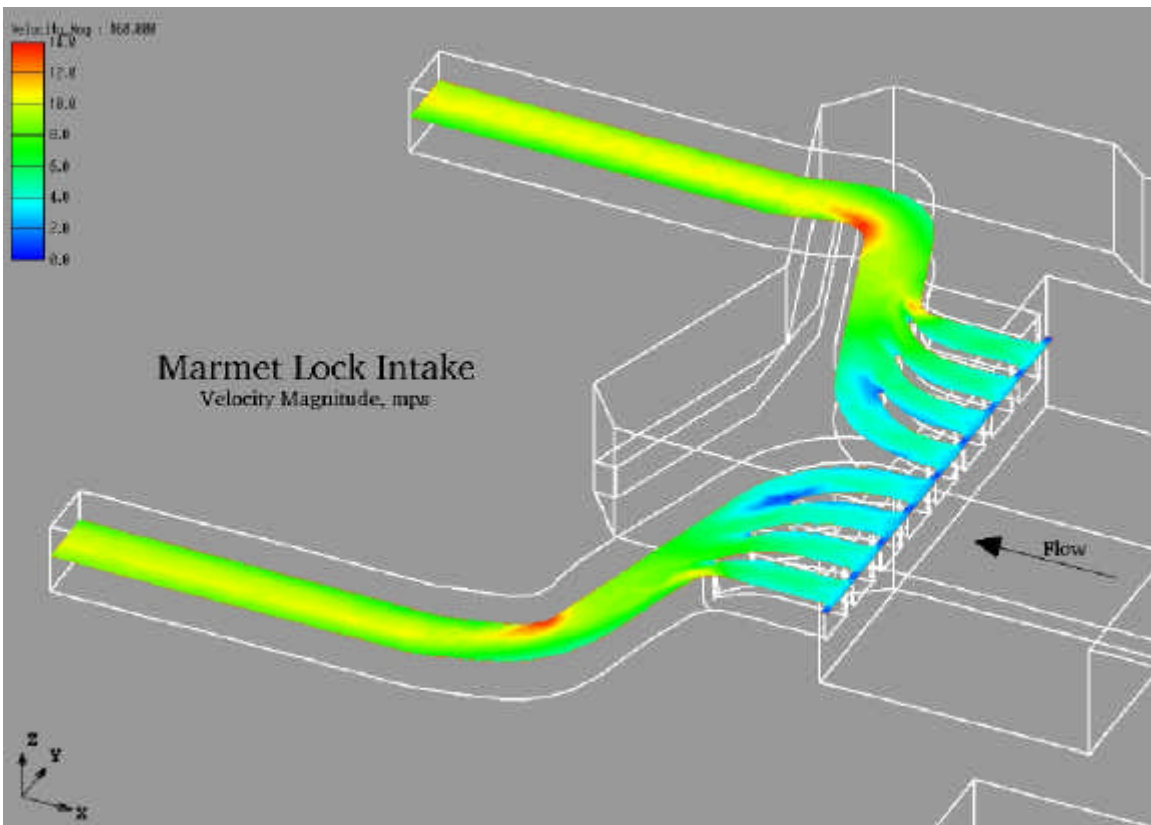


Figure 4. Velocity contours on a plane through center of intake and culverts

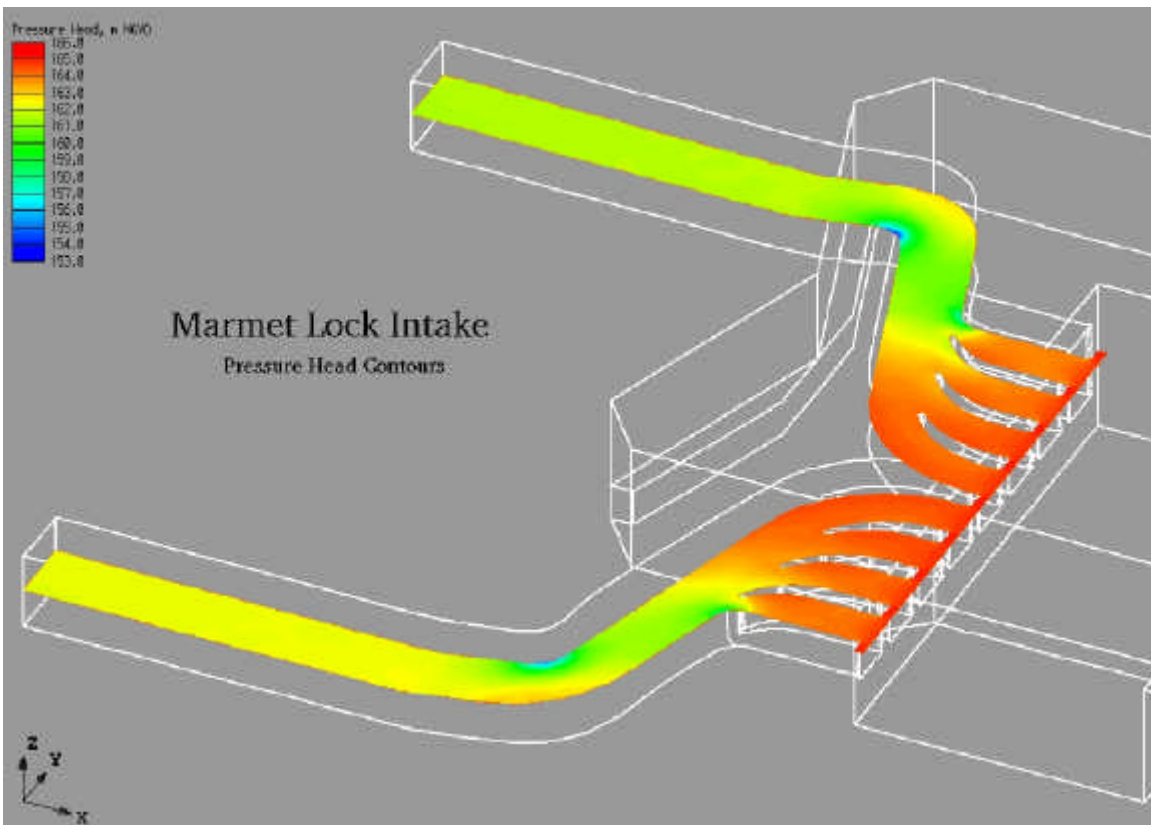


Figure 5. Pressure contours on a plane through center of intake and culverts

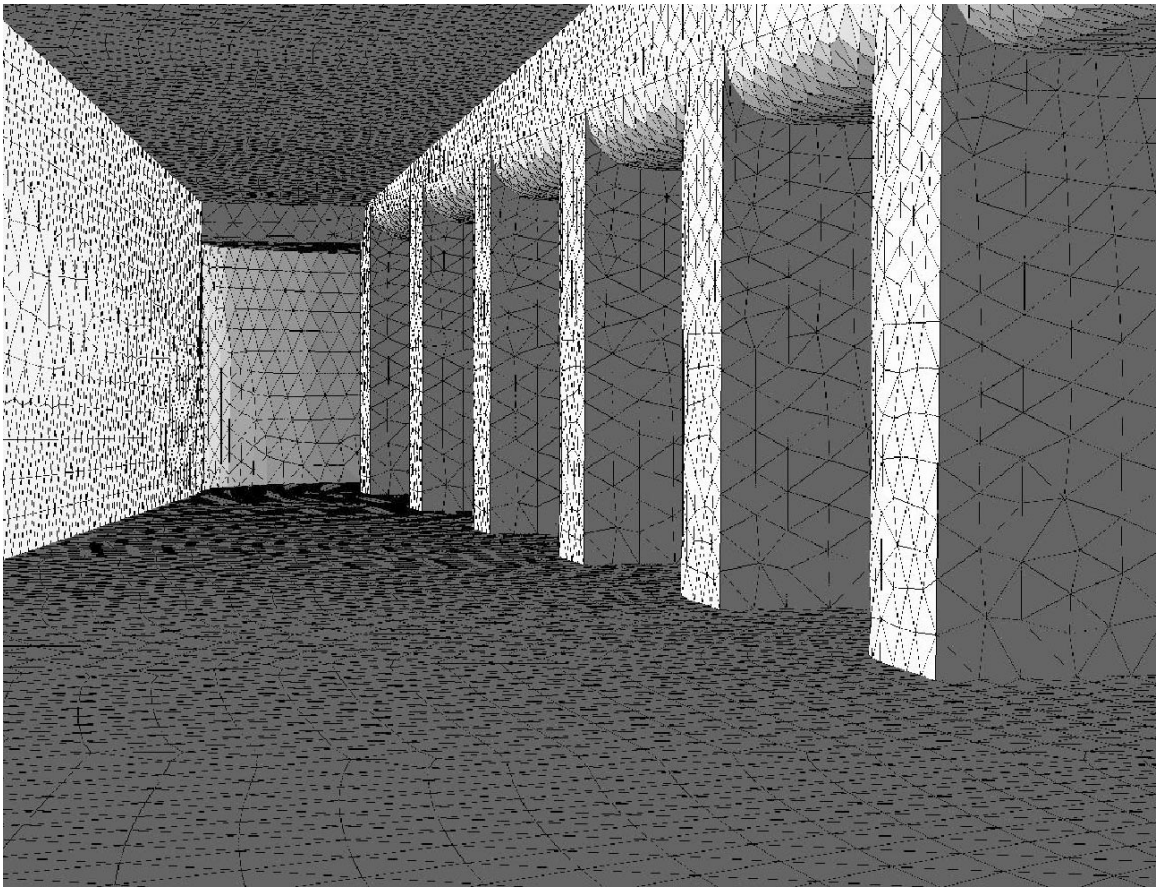


Figure 6. Surface mesh inside multiported outlet

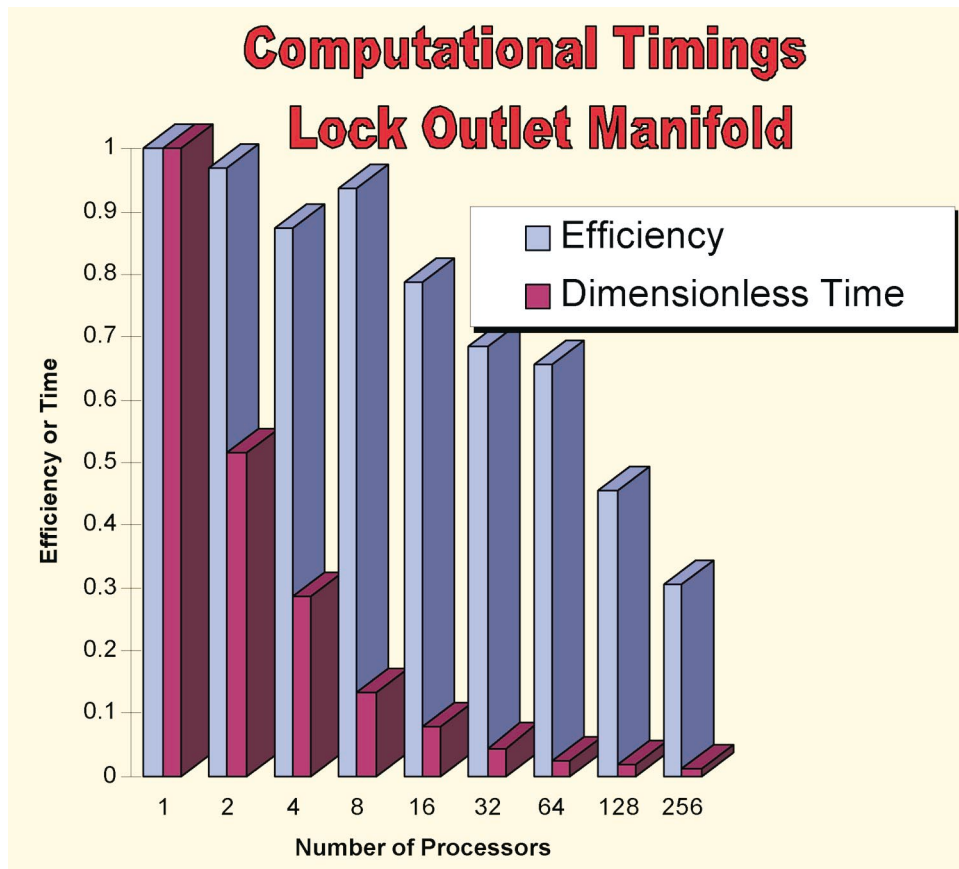


Figure 7. Computational timings for lock outlet manifold model

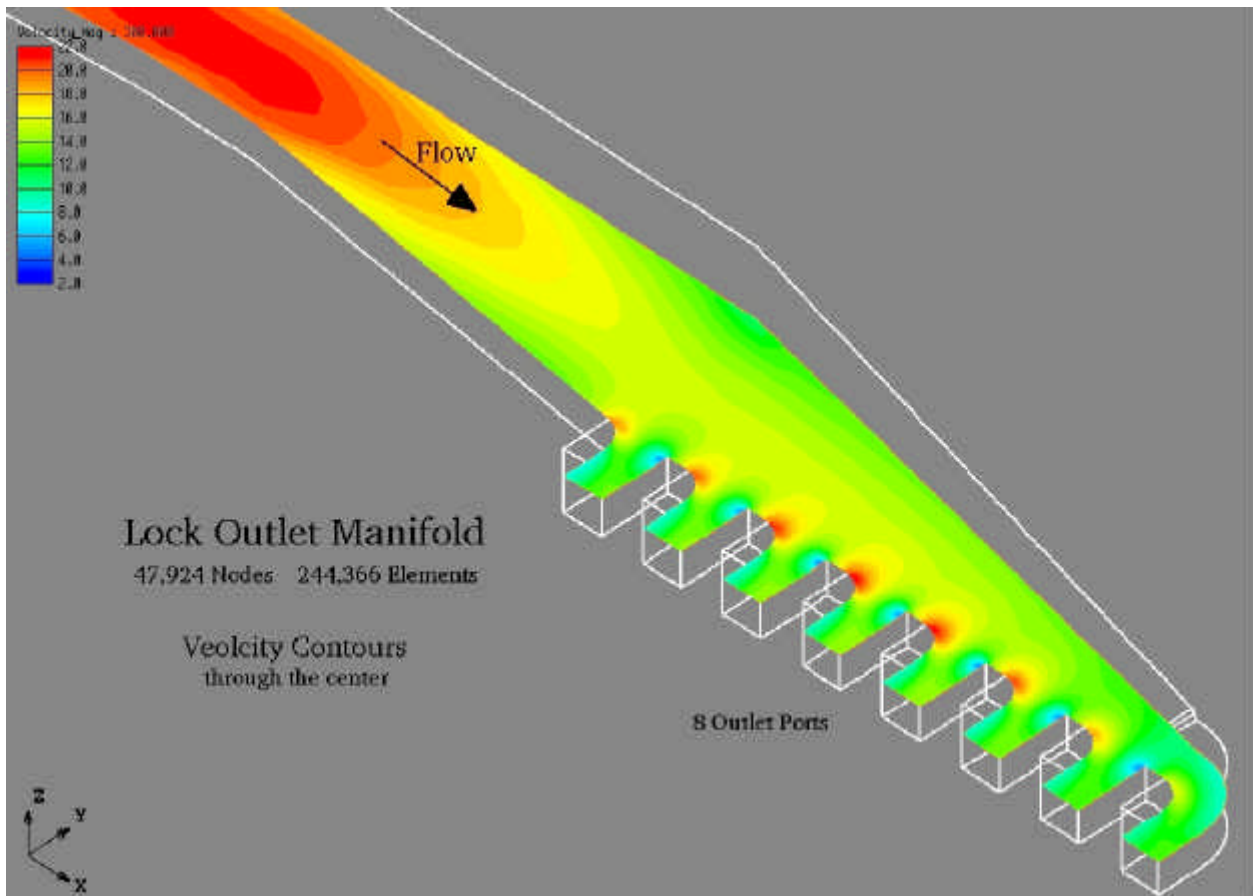


Figure 8. Velocity contours on a plane through center of outlet manifold

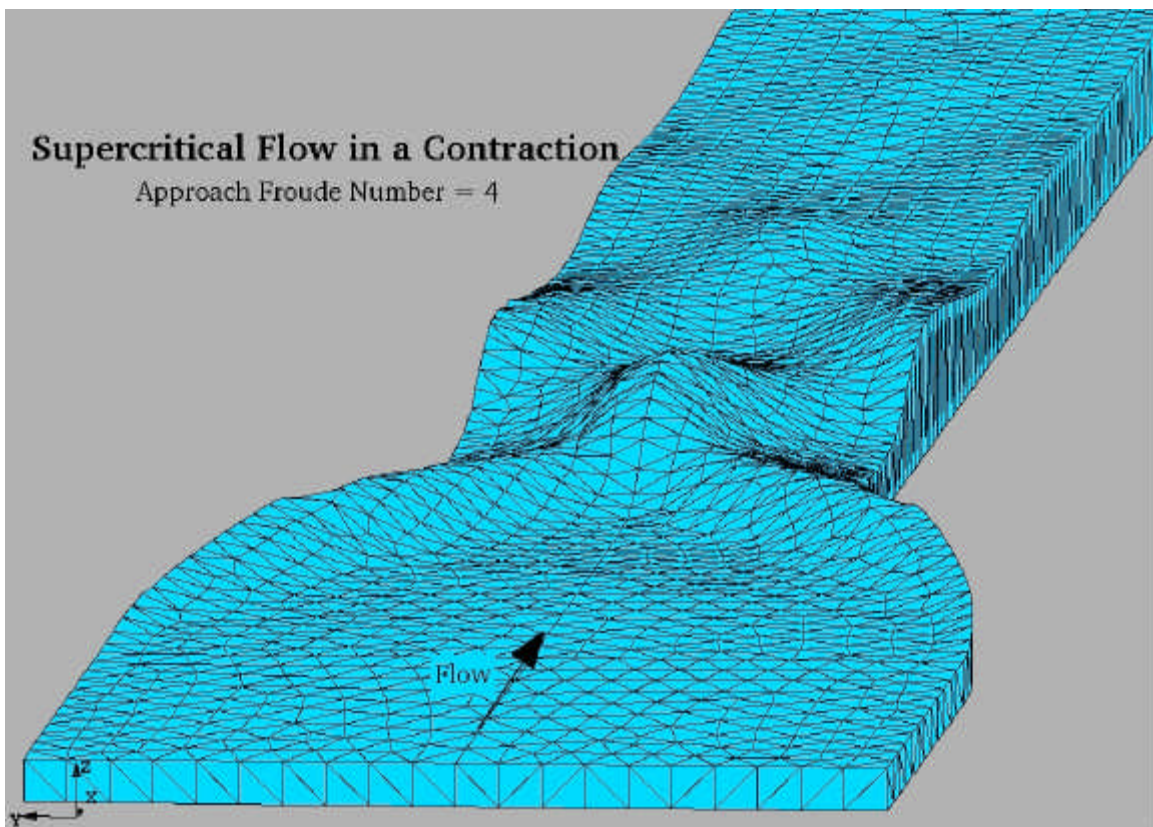


Figure 9. Computational mesh resulting from supercritical flow in a contraction

Entrance Channel Oscillations, Willapa Bay, Washington

Edward B. Hands¹ and Vladimir Shepsis²

Abstract

Navigation through Willapa Bay, WA, is complicated by constantly changing alignments and positions of the main entrance channel. Massive sediment movement in the entrance correlates with El Niños. When spit elongation deflects the channel and other conditions are met, El Niño-related processes seem to trigger a new outlet. The primary factors in addition to El Niño are ebb channel inefficiencies, rates of spit extension and erosion, and sediment recycling within the entrance. Though inlet dynamics are not among the many phenomena already linked to El Niños, this coupling, if valid for Willapa Bay, should apply to certain other inlets worldwide. Understanding how channels respond to quasi-predictable phenomena will improve guidance for management of the affected inlets. This article was extracted from Hands and Shepsis (1999).

Willapa Bay

Willapa Bay is the second largest bay on the Pacific Coast of the United States after San Francisco Bay. Willapa Bay lies approximately 45 km (28 miles) north of the mouth of the Columbia River and 19 km (12 miles) south of the entrance to Grays Harbor (Figure 1). Willapa Bay has served oceangoing vessels for nearly two centuries, but passage in and out of the bay has always been treacherous due to intense waves and currents at its unstructured entrance. The constantly changing configuration of the channel further hinders navigation. In a single month, the outer channel

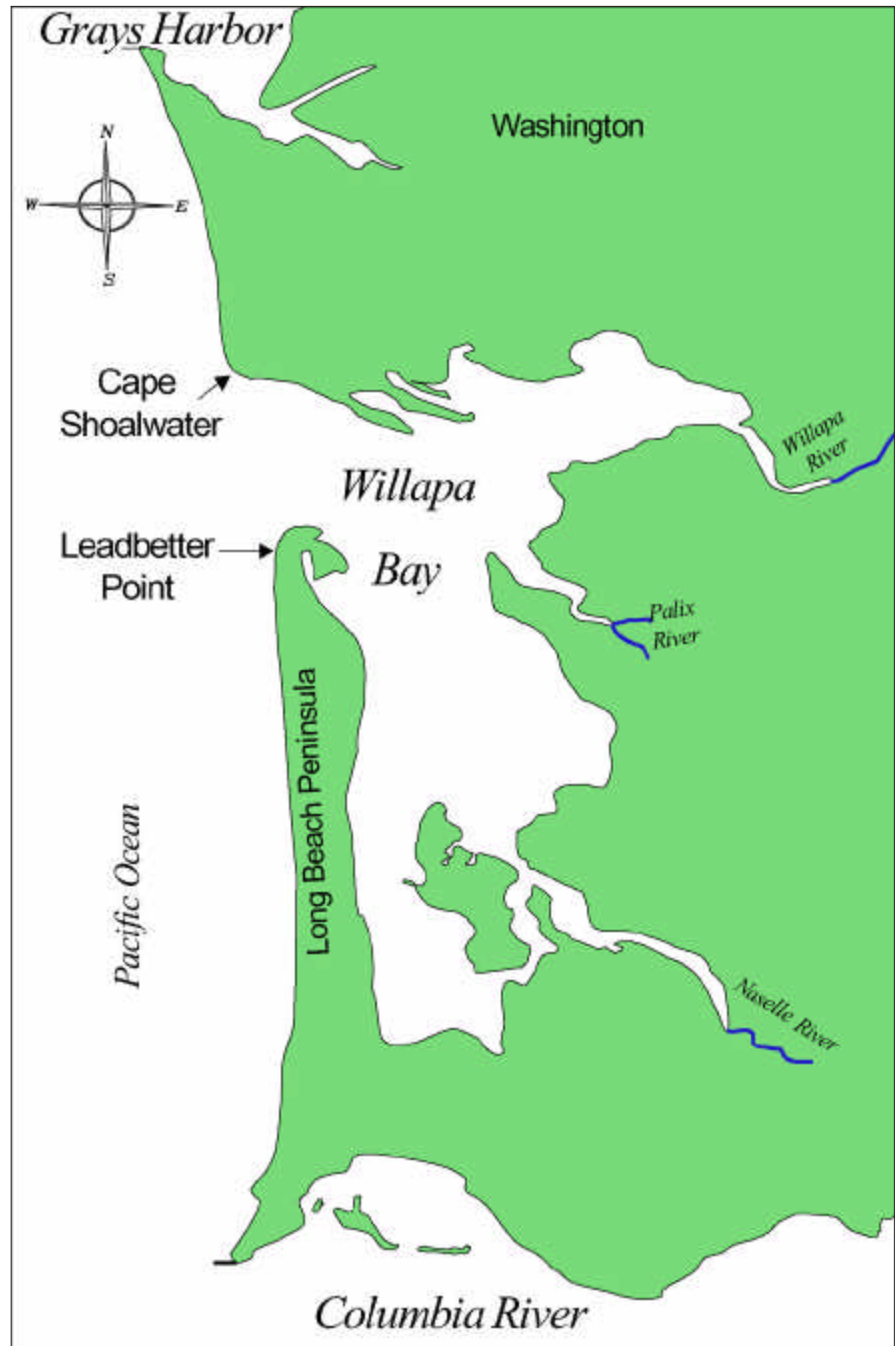


Figure 1. Location map

- 1 Research Scientist, U.S. Army Engineer Research and Development Center, 3909 Halls Ferry Road, Vicksburg, MS 39180-6199
- 2 Senior Scientist, Pacific International Engineering^{PLLC}, 144 Railroad Ave., Suite 310, Edmonds, WA 98020

often migrates 125 m (400 ft) along the coast. In storms, channels can move more than 300 m (1,000 ft) (Pacific International Engineering 1996). Net displacements over a decade are on the order of 6 km (20,000 ft). These morphologic changes, although large and complex, do include a long-term repeated pattern related to tidal shoal dynamics. Off Cape Shoalwater, a large submerged shore-tied spit grows southward from year to year along the outer margin of the ebb shoal. As the spit grows, it pushes the North Fairway channel ahead of it and deflects the channel orientation through 140 deg on a decadal scale. During evaluation of the feasibility of relocating the channel to a less dynamic part of the 11-km (7-mile)-wide entrance, an apparent correlation between cycles of channel reorientation and past El Niño Southern Oscillation (ENSO) events was identified.

Bay Hydrodynamics

The Willapa Bay entrance is composed of broad, shallow to supratidal flats dissected by a system of tidal channels. In different years, there have been as many as three major tidal channels through the entrance. These channels fall into three regions referred to as North, South, and Middle Fairways (Figure 2). For at least the last 146 years, the channel in the North Fairway has always captured the majority of the bay's tidal discharge.

Jarrett (1976) reports that Willapa Bay's tidal prism is about $6 \times 10^8 \text{ m}^3$ ($2 \times 10^{10} \text{ ft}^3$) making it one of the largest in the continental United States. Willapa's prism-to-bay volume ratio is also extremely large. About 45 percent of the below-mean-sea-level bay volume is exchanged during each tidal cycle. This large tidal prism enters and exits the bay twice daily, creating powerful currents that reach 2.5 to 3.0 m/sec (5-6 knots) on a regular basis and 4.5 m/sec (8 knots) during extreme tides. Preliminary estimates of peak discharge, based on recent acoustic-doppler current profiles, are about $33,500 \text{ m}^3$ ($43,800 \text{ yd}^3$) per

second during a 3-m (10-ft) fall of tide (Kurrus et al. 1999).

Crossing the entrance, one encounters large unbroken waves, breakers, and reformed ocean waves. Wave action in the entrance is complicated by superposition of local wind waves generated over the sizable inner bay on top of the ocean waves traveling along the channel, and ocean waves refracted and transformed over the channel-margin shoals. Winter is the season of the highest and longest-period ocean waves (heights often near 8 m or 26 ft, with periods near 13 sec, occasional heights over 10 m). These large winter waves arrive from the southwest. Summer waves are smaller ($\approx 2 \text{ m}$ or 6 ft), and arrive out of the north. Thus, the net longshore transport is directed northward along the open coast.

Bathymetric Database

The bathymetric data were extracted from the U.S. Army Engineer District, Seattle, archives and combined with recent surveys completed under a new Willapa Navigation Channel Feasibility Study (Kraus, editor, 2000). The early U.S. Coast Survey and the Seattle District conducted hundreds of hydrographic surveys of Willapa Bay over the last century and a half. Sixty historical charts were selected to represent changes from 1852 to 1985. The more recent years were represented using the Corps' digital data from 1993, 1996, 1997, and 1998. Supplementary information on shoal positions was taken from a set of high-altitude images covering the years 1950-1998.

The Corps of Engineers dredged the entrance from 1931 to 1941, 1949 to 1974, and in 1997, to create a small test channel in the Middle Fairway. This maintenance dredging typically removed less than $268,000 \text{ m}^3$ ($350,000 \text{ yd}^3$) per dredging year. A total of $4.3 \times 10^6 \text{ m}^3$ ($6 \times 10^6 \text{ yd}^3$) was dredged between 1951 and 1997.

Geomorphic Cycles

A compilation of 1:60,000-scale charts (U.S. Army Engineer District, Seattle, 1949) suggests there has long been an awareness that Willapa channels follow a pattern, even though this did not appear in the early published literature. Andrews (1965) and Terich and Levenseller (1986) pointed out that the channel migrates southward, but documentation and analysis of this pattern was still lacking. Recent inspection of the bathymetry record allows full documentation (at 1-year intervals) of five complete cycles of spit dissection and channel migration between 1941 and 1999. Additional cycles are indicated in the earlier part of the record, where they are less fully recorded because surveys were conducted less frequently prior to 1920.

In 1887, a prominent submerged spit extended south and oceanward from Cape Shoalwater. Growth of this spit deflected the North Channel discharge from just off Cape Shoalwater to south of Leadbetter Point before allowing open communication between the North Channel and the ocean. When the submerged spit extends far to the south, (as it did then and repeatedly later) it is subject to breaching by a new outlet located near the north shore. The new outlet allows ebb currents to flow directly seaward. Eventually this northern outlet captures the majority of the tidal exchange. The distal remnant of the spit migrates southeastward as an isolated shoal, eventually merging with other bay-mouth shoals. The pattern repeats itself as the spit grows and deflects the North Channel to the south again.

The southernmost channels tend to be best developed about a quarter of the way into the spit extension cycle. Spit dissection starts at one to four locations. Erosion of the new outlets always begins on the landward side of the spit, presumably where acceleration of the discharge peaks because the flow must either turn along the spit or increase speed over it. Several years of seaward cutting are typically necessary before one of the new outlets

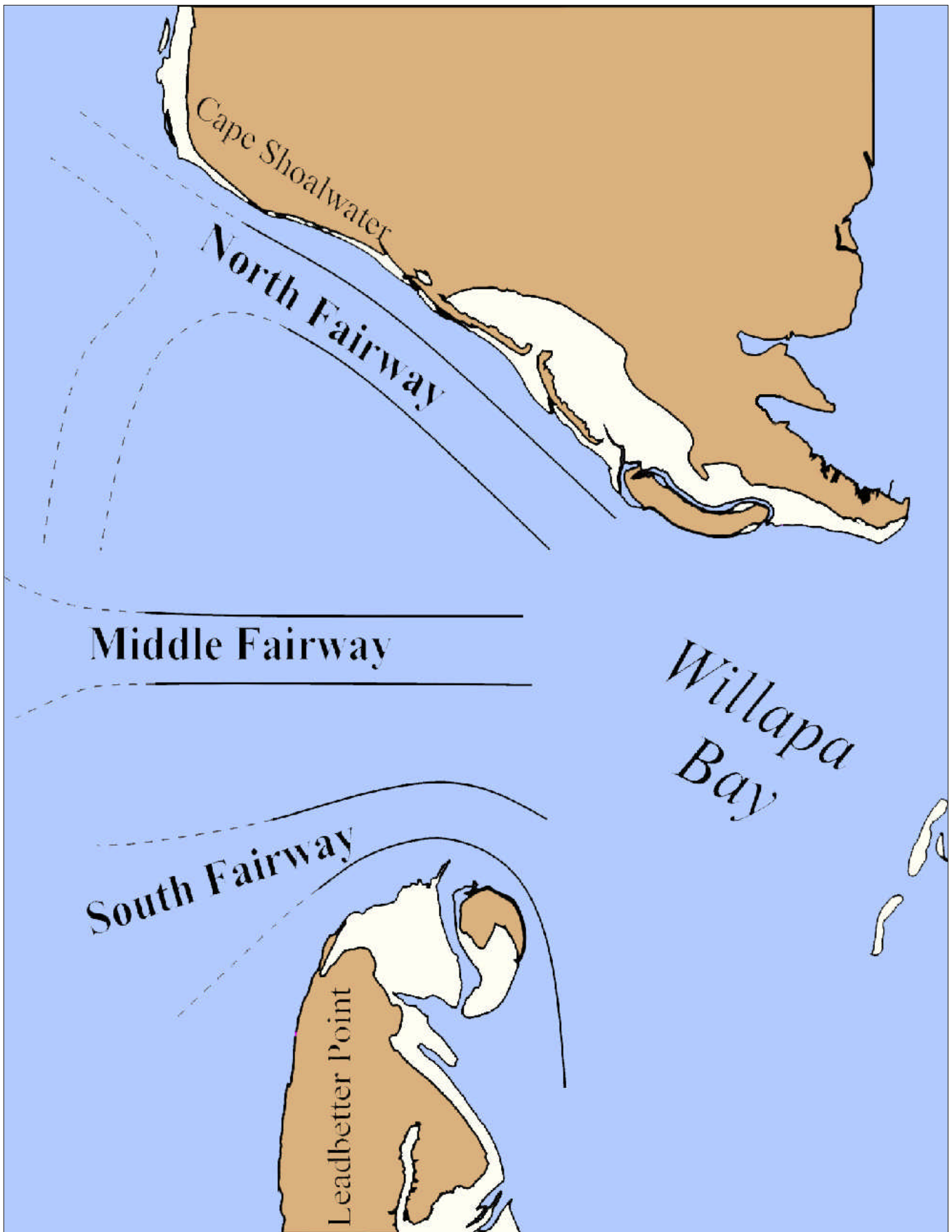


Figure 2. Fairways schema (loci of historic channels)

captures the majority of the North Channel discharge; then the other outlets shoal. The outlet that prevails is usually the one located near latitude $46^{\circ} 43' N$, not where the freeboard over the spit is greatest, but where the momentum of ebb flow against the spit is highest. Though the older, still dominant, outlet may have an azimuth less than 180 deg, the new outlet that will prevail has an azimuth greater than 270 deg.

Figure 3 illustrates part of one of these cycles starting with initial dissection of a mature submerged spit

in 1941, through shoal isolation in 1945, and merging of the spit-derived shoal with inner mouth shoals in 1949. The next northern outlet began to cut directly seaward at the same location in 1954. The details of the five cycles documented thus far are illustrated in 1-year increments in Hands (2000). The duration of the cycles varied from 8 to 27 years. The northern root of the spit never was without a supply of sand. So, the shore-tied spit continually pushed southward repeatedly deflecting the main

channel into a hydraulically inefficient, almost north-south orientation.

Timing of Climatic and Geomorphic Events

The sstoi index is a sea surface temperature anomaly for various areas of the equatorial Pacific calculated by the National Oceanic and Atmospheric Administration's (NOAA) Climate Prediction Center. Monthly sstoi indices for East Pacific region Nino 1+2 (0-10S, 90W-80W) are shown as points in Figure 4 together with a smoothed curve fit to this data. Positive anomalies indicate unusually warm water. So, according to this index, periods when the curve is above zero correspond to El Niños. The sstoi time series dates back only to 1950.

Willapa charts clearly display two earlier complete episodes of channel realignment that began in 1933 and 1941 before the earliest sstoi index. So, in the lower half of Figure 4, a second El Niño index is plotted. This second index was developed by Quinn et al. (1978). For his purpose, precision was less important than obtaining a comprehensive long-term index. So, Quinn derived an index that combined many factors and sources of information on global pressure systems and coastal South American rainfall, fisheries, sea surface temperatures, and sea bird reports dating back to the 1700s. Quinn's index is widely cited by climatologists and even used by coastal engineers (e.g., Seymour 1998). Quinn's index is adopted here to investigate the earlier episodes of channel reorientation.

Quinn's index does not specify the month of initiation and the duration of El Niños. A modification was adapted for use in Figure 4 that represents the time and intensity of Quinn's index with bars. The bars were centered on December 31 because the typical El Niño causes warmest water temperatures in the tropical east Pacific during the Northern Hemisphere's winter. Bar widths were arbitrarily set to span the six months from October 1 to March 31. The actual onset and duration of El Niños varies as

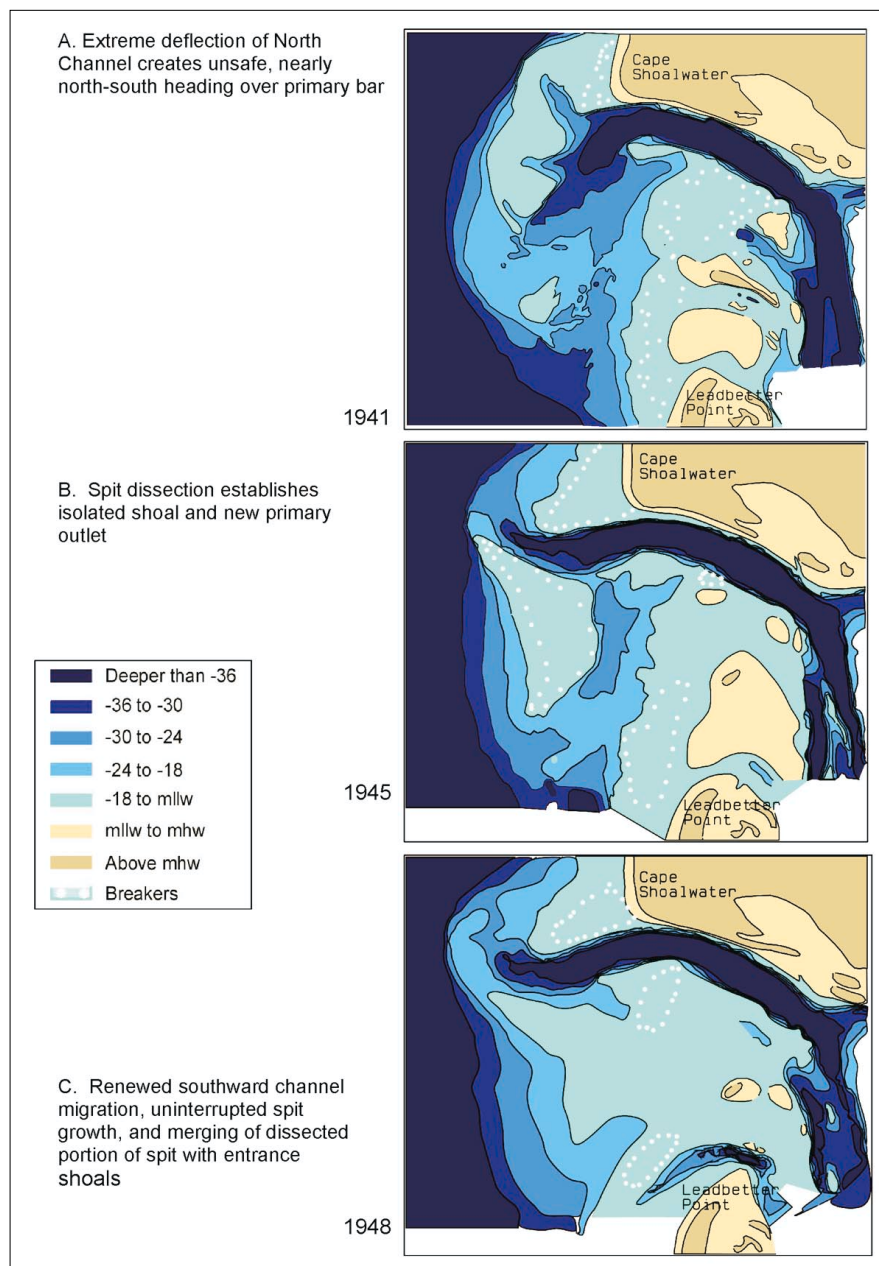


Figure 3. One half of the geomorphic cycle

indicated by changes in peaks of the smoothed sstoi curve. Heights of the bars reflect Quinn's intensity categories. Pre-1980 gaps between the bars indicate low intensity El Niño-, neutral-, or La Niña-years. Note that where they overlap, all of Quinn's bars align with a peak in the sstoi index. All channel reorientations began during an El Niño time.

A specific year was assigned to the initiation of each channel orientation based primarily on analysis of charted bathymetry. Each primary North Channel was traced back to its first appearance as a small outlet on an annual chart (i.e., the prior year chart would have no indication that a new outlet was being cut). The bars indicating initiation of a new cycle in Figure 4 have a left edge aligned with mid-October (end of the survey season) of the year preceding outlet recognition and a right edge aligned with the following mid-October. The bar thus spans the 1-year period during which erosion of the new outlet started. With one exception, the year of the earliest chart depicting a new outlet was

selected to indicate the beginning of a new channel cycle. The exception was for 1969. The main outlet of the 1980s can be traced back to a large secondary outlet on the 1971 chart, a minor niche on the 1970 chart, and complete absence of any outlet on the 1969 chart. Though not really an outlet, the 1970 niche was interpreted as the beginning of the next cycle because it was in the position where a sizable outlet was charted the next year, and also because the October 1969 aerial photographs reveal at that location a substantial gap in a line of breakers outlining the spit. Only a niche had been charted in the summer of 1970, but the gap in the breakers on the mid-October 1969 aerials, indicated initiation of the new outlet had begun. This is the only instance where initiation of the new outlet was not clear on the annual bathymetric chart for the indicated year.

Figure 4 thus reveals a strong correlation between channel reorientation and El Niños. Less than half of the El Niños, however, were

accompanied by channel reorientations. If spit elongation reaches an unstable stage, then El Niño-related conditions seem to increase the chance that a breach will be initiated. Spit elongation is the more basic prerequisite, perhaps because it creates an increasingly unstable constraint on the ebb jet, which has already been forced westward by confrontation with the northern bay shore.

Conclusions

Historically, initiations of major realignments of the Willapa Channel coincide with El Niño conditions in the tropics. The time that elapses between initiation and the full development of a new outlet is longer than the El Niño perturbation. A six-month relaxation time for a small initial cut into the landward side of the spit is, however, consistent with forcing by El Niño. There are many more El Niños than channel cycles. A conceptual framework guiding further investigation of this cycle consists of three processes-response

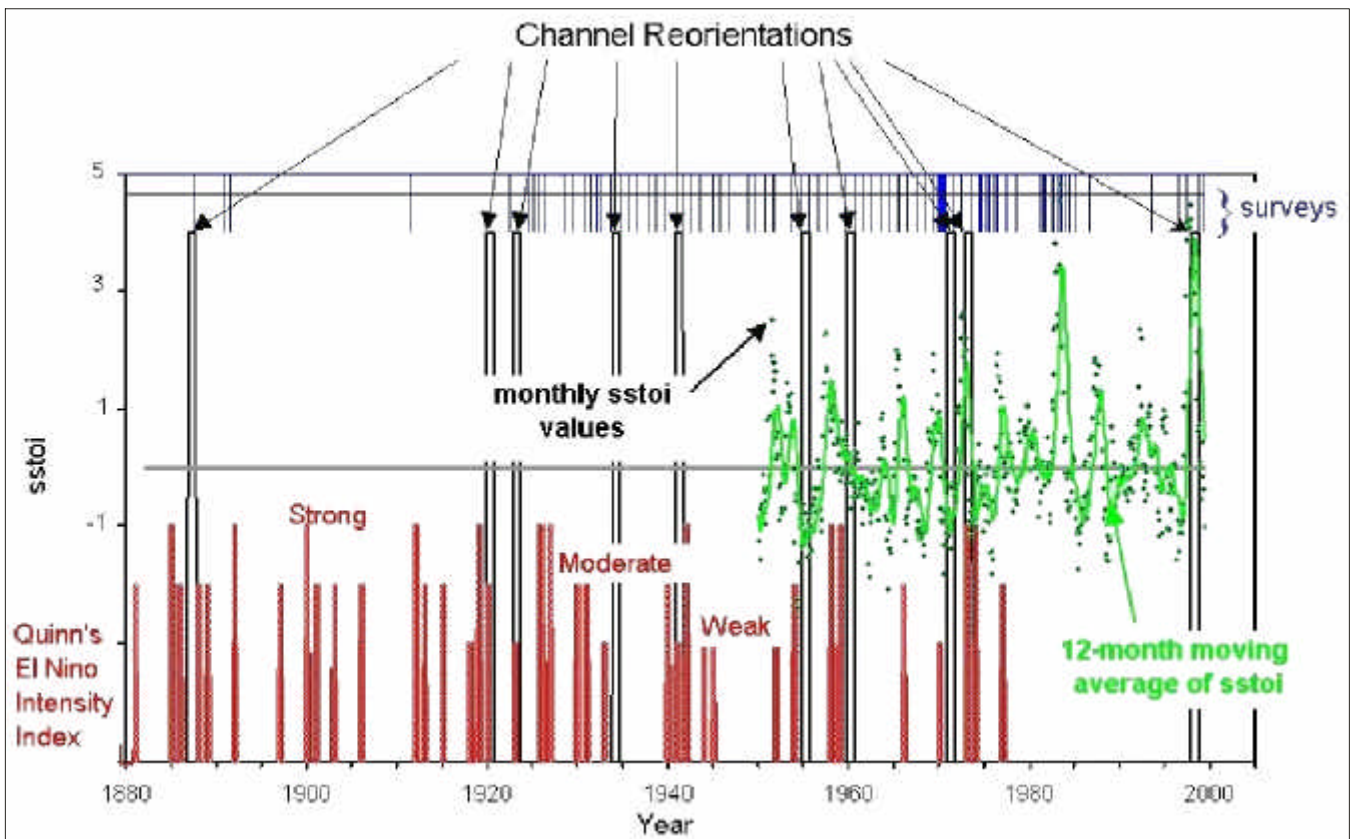


Figure 4. Coincidence of El Niño and channel reorientations

couplings at different time-space scales.

First, deflection of the North Channel to a nearly north-south alignment is a prerequisite for initiation of a viable new outlet by processes that act over a period of months related to El Niño. Once initiated, if the outlet is near 46° 43' N latitude and has an azimuth greater than 270 deg, it will continue to deepen, widen, and extend seaward.

Outlet expansion continues for several years until it completely dissects the Cape Shoalwater submerged spit and captures the primary tidal flow in and out of the North Channel. During this 2- to 4-year phase, the principal forces are the momentum of ebb currents and the greater hydraulic head across the spit rather than along the north-south outlet.

The third phase is persistent southward channel migration, which lasts 10 to 30 years. Investigation of this longest phase will concentrate on processes controlling sediment recycling within the entrance and possible local reversal of longshore transport toward the entrance from the north shore.

The ability to predict natural interannual channel cycles would expand the potential economic strategies for maintaining safe inlet navigation. Until the mechanisms connecting El Niño to local hydrodynamics are better known, however, too many uncertainties exist to presently rely on forecasts of remote phenomena to predict a new cycle at Willapa Bay.

Acknowledgements

An agreement between the U.S. Army District, Seattle, and the Port of Willapa Harbor to participate in the Willapa Channel Feasibility Study made this research possible. Assistance in this investigation by Evan Hamilton, Inc. and Pacific International Engineering, Inc. is gratefully acknowledged.

References

- Andrews, R. S. (1965). "Modern sediments of Willapa Bay, Washington: A coastal plain estuary," TR 188, Department of Oceanography, University of Washington, Seattle, WA.
- Hands, E. B. (2000). "Study of navigation channel feasibility, Willapa Bay, Washington, Chapter 3: Geomorphology," Edited by N. C. Kraus, ERCD/CHL TR-00-6, U.S. Army Engineer Research and Development Center, Vicksburg, MS.
- Hands, E. B., and Shepsis, V. (1999). "Cyclic channel movement at the entrance to Willapa Bay, Washington, USA," Proceedings, Coastal Sediments '99. American Society of Civil Engineers, Hauppauge, Long Island, NY, 2, 1,522-1,536.
- Jarrett, J. T. (1976). "Tidal prism-inlet area relationships," GITI Report 3, U.S. Army Engineer Waterways Experiment Station, Vicksburg, MS.
- Kraus, N. C. (1998). "Inlet cross-sectional area calculated by process-based model." Proceedings, International Conference on

Coastal Engineering. American Society of Civil Engineers, Copenhagen, Denmark, 3, 3,265-78.

- Kraus, N. C., editor. (2000). "Study of navigation channel feasibility, Willapa Bay, Washington." ERDC/CHL TR-00-6, U.S. Army Engineer Research and Development Center, Vicksburg, MS.
- Kurras, K., Titus, C., FitzGerald, K., and Giles, S. (2000). "Study of navigation channel feasibility, Willapa Bay, Washington, Chapter 4: Field data collection and analysis." Edited by N. C. Kraus. U.S. Army Engineer Research and Development Center, Vicksburg, MS.
- Pacific International Engineering. (1996). "Willapa Bay channel restoration project, Pacific County, Washington," Contract Report, PIE, Inc., Seattle, WA.
- Quinn, W. H., Zopf, K. S., Short, K. S., and Kuo-Yang, R. T. W. (1978). "Historical trends and statistics of the Southern Oscillation, El Niño, and Indonesian droughts," *Fisheries Bulletin*, 76, 665-73.
- Seymour, R. J. (1998). "Effects of El Niño on the west coast wave climate," *Shore & Beach*, 66 (3), 3-6.
- Terich, T., and Levenseller, T. (1986). "The severe erosion of Cape Shoalwater, Washington," *Journal of Coastal Research*, 2 (4), 465-77.
- U.S. Army Engineer District, Seattle. (1949). "Willapa Harbor, Washington: Surveys of bar channels from 1852 to 1931," File E/4/2/49, Seattle, WA.

Wave Damage on Rubble-Mound Breakwaters

J. A. Melby¹ and N. Kobayashi²

Abstract

Physical-model laboratory experiments are described consisting of seven relatively long-duration rubble-mound breakwater damage test series which were conducted in a flume using irregular waves. New damage measurement techniques were developed, and damage development data were acquired for breaking wave conditions. Wave height, wave period, water depth, storm duration, storm sequencing, and stone gradation were all varied systematically. The experiment yielded relationships for both temporal and spatial damage development although only the spatial aspects are described herein. It is shown that the damaged profile can be described by the eroded area A_e , maximum eroded depth d_e , minimum cover depth d_c , and maximum eroded length l_e . These parameters are normalized as $S = A_e/D_{n50}^2$, $E = d_e/D_{n50}$, $C = d_c/D_{n50}$, and $L = l_e/D_{n50}$, and the mean and standard deviation of each are shown to be a function of the mean damage \bar{S} . This article is extracted from Melby and Kobayashi (1999).

Introduction

Contemporary rubble-mound breakwater armor stability design is founded on the well-known works of Iribarren and Hudson conducted over several years. Much work has been done to extend these stability models for no-damage design conditions, but little work has been done to quantify damage progression. With only limited knowledge of damage progression, it is difficult to rationally determine life cycle costs

or to evaluate and prioritize maintenance requirements for various projects. Further, determining the reliability with adequate accuracy for a particular design is impossible without prediction models for damage progression.

Existing stability formulas are limited to constant wave conditions [e.g., Hudson (1959) and van der Meer (1988)]. They are primarily intended to give a stable armor layer for a design-level storm. These existing formulas can be used to design a new armor layer, but are not sufficient to predict life-cycle costs or to determine maintenance requirements for damaged rubble mounds. Van der Meer (1988) showed that the shape of the eroded profile may be important in assessing the remaining capacity of an armor layer. Mansard et al. (1996) utilized the minimum cover layer thickness to describe failure of an armor layer. Melby and Kobayashi (1998a, 1998b) showed that this cover layer thickness as well as the depth and extent of erosion can be used to characterize the profile, and all are quite variable along the slope.

Physical Model Experiments

Physical model experiments were designed to provide the basis for an empirical model for spatial and temporal breakwater damage development. The experimental design was focused on quantifying damage for long duration tests composed of sequences of storms. The objectives of the experiments were to (a) quantify the progression of damage for

multiple storm events, with water level, breaking wave height at the toe, and storm duration being the primary variables (wave period and stone gradation were also varied systematically), (b) quantify the uncertainty or scatter in damage due to natural variability, and (c) determine whether the ordering of storm events affects the ultimate damage level.

The experiments utilized two rubble-mound breakwater sections in a wave flume. Figure 1 shows the flume profile, and Figure 2 shows a typical structure cross section. A total of seven irregular wave test series were conducted, shown in Table 1. Each series was composed of a sequence of storms of varying wave height and water level. Parameters varied systematically from series to series were storm duration, storm ordering, wave height, water depth, wave period, and armor gradation. The structures were profiled using a newly developed automated profiler (Winkelman 1998). The profiles were used to determine the eroded cross-sectional area and profile characteristics.

The experiment was conducted in a 61-m-long by 1.5-m-wide by 2-m-deep flume, with a beach slope of 1V:20H. Two side-by-side identical conventional rubble-mound cross sections were constructed with seaward slopes 1V:2H, crest heights 30.5 cm, and angular armor stone. Irregular waves corresponding to the Texel, Marsen, Arsloe (TMA) spectrum were run in bursts of 15 min. The undamaged underlayer and armor layer for the two identical structures were profiled before each series. Then both structures were

1 Research Engineer, U.S. Army Engineer Research and Development Center, Coastal and Hydraulics Laboratory, Vicksburg, MS 39180

2 Professor and Associate Director, Center for Applied Coastal Research, University of Delaware, Newark, DE 19716

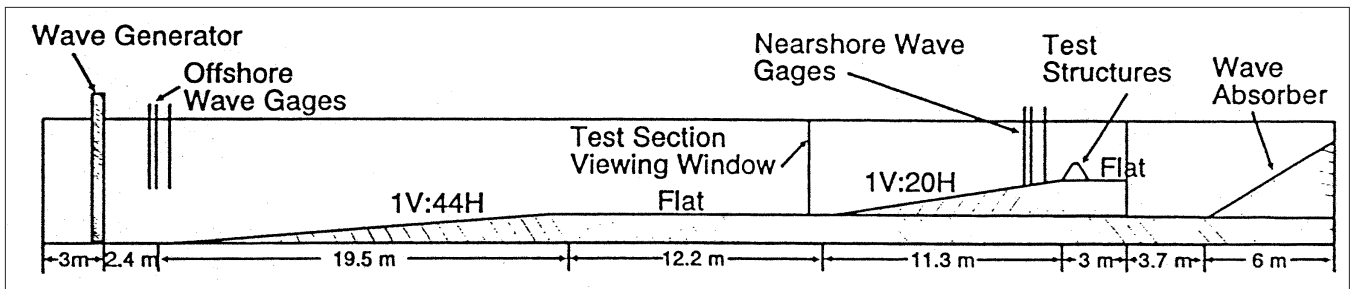


Figure 1. Experimental wave flume profile

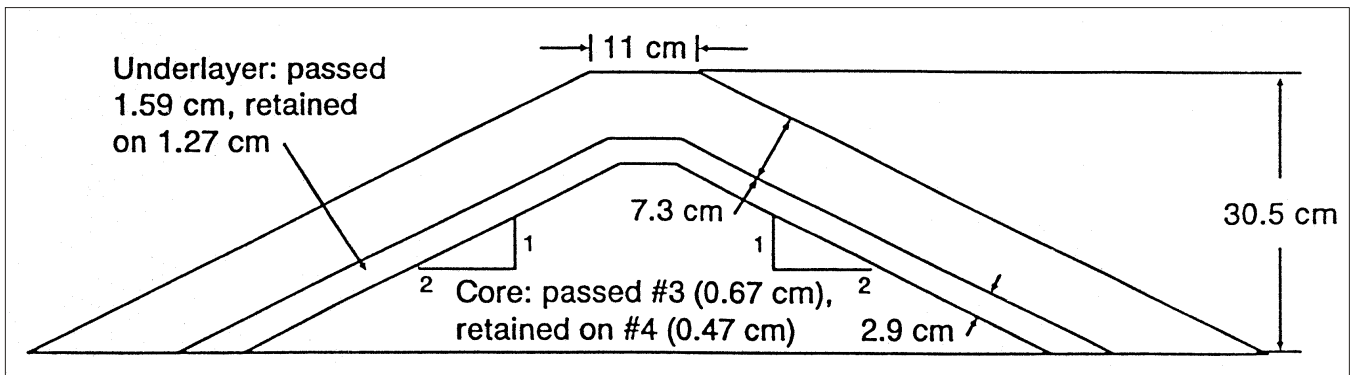


Figure 2. Model structure cross section for uniform stone

profiled after each 30 min of irregular waves.

The seven test series were designed to define spatial and temporal damage development under irregular depth-limited breaking wave conditions. Series A', lasting a total of 28.5 hr, was run until failure of the armor layer occurred, where failure was defined as exposure of the underlayer through a hole of diameter of at least D_{n50} . This series was intended to define the long-term response of a structure. Series A' was run once yielding 16 alongshore profiles every 30 min. Series B', C', D', E', F', and G', each lasting approximately 9 hr, were run twice producing 32 alongshore profiles per

30 min. These latter series were not run to failure, but were intended to define the damage development for various conditions. Series B' and C' were designed to investigate storm sequencing by running low water first then high water in B', and then reversing the water levels in C'. Series B', D', and E' investigated period effects, each having a different peak period. Series F' and G' investigated stone gradation effects. The average damage, \bar{S} , and the standard deviation of damage, σ_S , were computed using the 16 or 32 profiles after each 30 min of waves.

Two very different armor stone gradations were utilized. The armor stone for Series A', B', C', D', and

E' was uniformly sized with a median mass $M_{50} = 128$ g, nominal diameter $D_{n50} = (M_{50}/\rho_a)^{1/3} = 3.64$ cm, stone density $\rho_a = 2.66$ g/cm³, and $D_{85}/D_{15} = 1.05$, where D_{85} and D_{15} are the nominal diameters corresponding to 85 and 15 percent finer for the stone mass distribution, respectively. The armor stone for Series F' and G' was widely graded riprap with a median mass $M_{50} = 256$ g, nominal diameter $D_{n50} = (M_{50}/\rho_a)^{1/3} = 4.58$ cm, stone density $\rho_a = 2.66$ g/cm³, and $D_{85}/D_{15} = 1.53$. The riprap followed the widest recommendation of the *Shore Protection Manual* (1984) of approximately $0.125M_{50} < M < 4M_{50}$. For all series, the underlayer had a gradation of $D_{85}/D_{15} = 1.32$ and was sized such that $(M_{50})_{armor}/(M_{50})_{filter} = 25$ and $(D_{50})_{armor}/(D_{50})_{filter} = 2.9$.

Damage can be defined according to Broderick and Ahrens (1982) as

$$S = \frac{A_e}{D_{n50}^2}$$

where A_e = eroded volume per unit length or cross-sectional eroded area (Figure 3). The eroded area was measured using a profiler composed of eight rods which spanned a width on one 35-cm structure. The alongshore profiler rod spacing was 5 cm.

Table 1. Summary of Test Series

Test Series	Test Type	Armor Type	Water Level Order	Test Duration, hr
A'	Deterioration to Failure	Uniform	Low - High	28.5
B'	Storm Ordering	Uniform	Low - High	8.5
C'	Storm Ordering	Uniform	High - Low	9.0
D'	Wave Period	Uniform	Low - High	8.5
E'	Wave Period	Uniform	Low - High	8.5
F'	Gradation	Riprap	Low - High	8.5
G'	Gradation	Riprap	Low - High	8.5

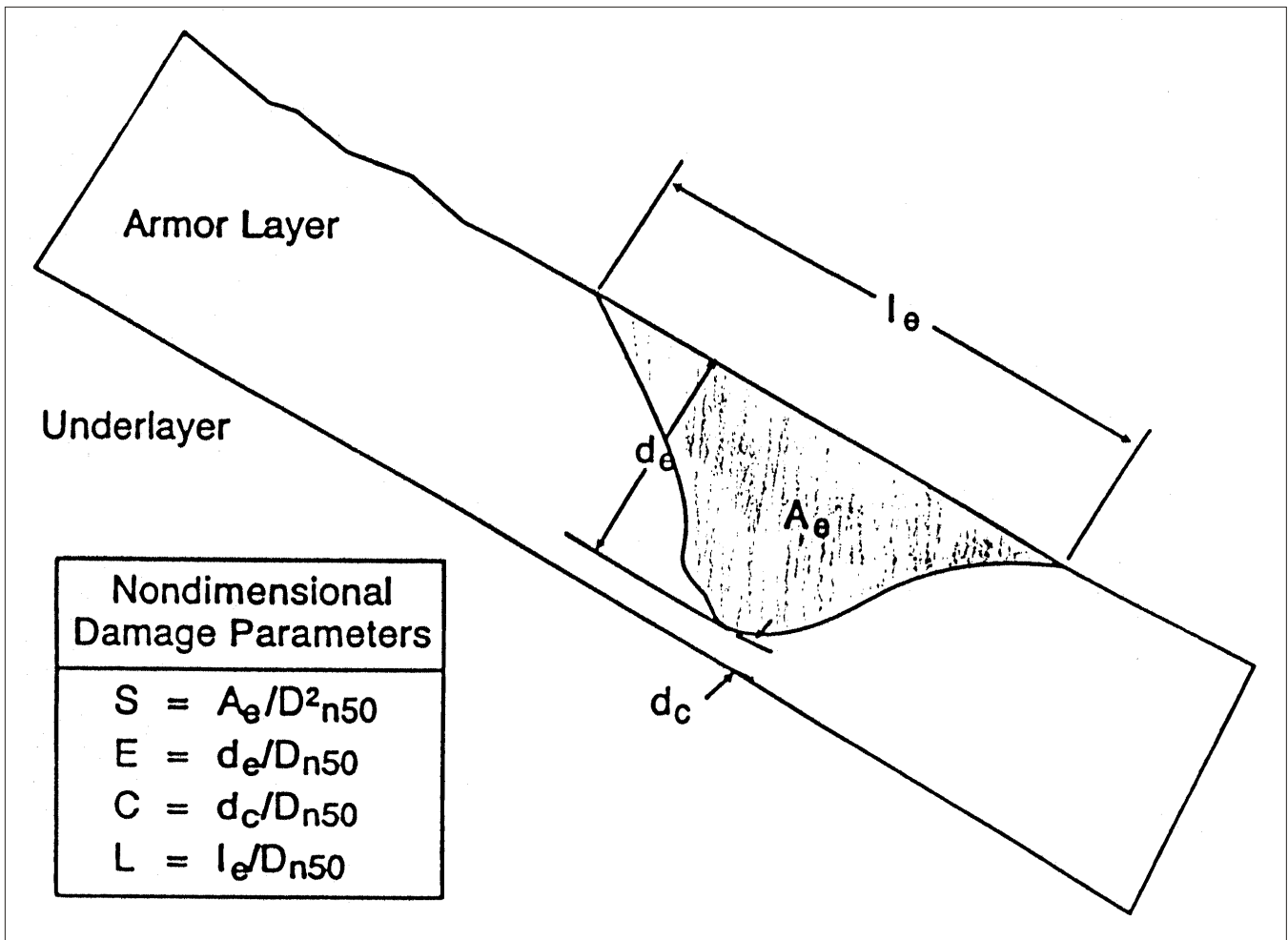


Figure 3. Breakwater profile with definition of damage parameters

The width of one structure was 0.76 m so the profiled section did not include the sidewall effect. Each profile rod had a sphere of diameter 3.64 cm at the profiling end that followed the slope as the profiler was moved along the flume. The position of each sphere was determined from digital measurements of the angular rotation of each profile rod and translational position of the profile carriage. This technique provided an accurate and complete profile as the cross-shore spatial sampling interval was less than 1 mm. The profile points were averaged over a small cross-shore spatial interval in order to eliminate contributions to the eroded area from minor down-slope shifting of the armor layer.

The eroded depth d_e , eroded length l_e , and cover depth d_c were used to define the profile shape. The eroded depth d_e was computed for each profile as the maximum

distance between the eroded profile and the undamaged profile, measured normal to the structure slope. Similarly, d_c was computed as the minimum slope-normal difference between the undamaged underlayer slope and the damaged profile. The eroded length was defined as $l_e \approx 2A_e/d_e$ corresponding to a roughly triangular shaped region along slope. The profile parameters were normalized to generalize the test results, as $E = d_e/Dn_{50}$, $C = d_c/Dn_{50}$, and $L = l_e/Dn_{50}$. The mean values were computed and denoted as \bar{E} , \bar{C} , and \bar{L} .

Incident wave statistics for all series are listed in Table 2. For all tests, the structure toe water depths were limited to $h_t = 11.9$ and 15.8 cm. The combination of wave periods and water depths produced low depth-to-wavelength ratios which resulted in severely breaking waves at the toe of the structure, which is

typical of design conditions on most U.S. coastlines and represents the worst case for stability. In Table 2, T_p = spectral peak period, H_{m0} = spectral significant wave height defined as $H_{m0} = 4m_0^{1/2}$ with m_0 = zero moment of the incident wave spectrum, $R = [(m_0)_r/m_0]^{1/2}$ = average reflection coefficient, with $(m_0)_r$ = zero moment of the reflected wave spectrum, T_m = mean wave period, H_s = average height of the highest 1/3 of waves, $H_{1/10}$ = average height of the highest 1/10 of waves, and $H_{2\%}$ = wave height exceeded by 2 percent of the waves in the wave height distribution. Time domain statistics T_m , H_s , $H_{1/10}$, and $H_{2\%}$ were all computed from a zero-upcrossing analysis.

Results

Melby and Kobayashi (1998a, 1998b) showed that the number of

Table 2. Summary of Incident Wave Characteristics

Series	Wave	Duration, hr	Ht, cm	Tp, sec	Hmo, cm	R	Tm, sec	Hs, cm	H1/10, cm	H2%, cm
A'	1	1.5	11.9	2.48	9.78	0.46	1.76	9.38	11.50	12.80
	2	1.5	11.9	2.48	12.40	0.47	1.69	11.60	13.80	15.37
	3	7.5	11.9	2.48	14.20	0.48	1.74	13.20	15.70	17.30
	4	1.0	15.8	2.59	10.50	0.52	1.73	10.10	12.72	14.30
	5	6.0	15.8	2.59	13.60	0.51	1.67	13.00	15.97	17.80
	6	11.0	15.8	2.59	15.80	0.51	1.66	14.90	18.00	19.30
B'	1	0.5	11.9	2.48	9.78	0.46	1.76	9.38	11.50	12.80
	2	2.0	11.9	2.48	12.40	0.47	1.69	11.60	13.80	15.37
	3	2.0	11.9	2.48	14.20	0.48	1.74	13.20	15.70	17.30
	5	2.0	15.8	2.59	13.60	0.51	1.67	13.00	15.97	17.80
	6	2.0	15.8	2.59	15.80	0.51	1.66	14.90	18.00	19.30
	C'	4	1.0	15.8	2.59	10.50	0.52	1.73	10.10	12.72
5		2.0	15.8	2.59	13.60	0.51	1.67	13.00	15.97	17.80
6		2.0	15.8	2.59	15.80	0.51	1.66	14.90	18.00	19.30
2		2.0	11.9	2.48	12.40	0.47	1.69	11.60	13.80	15.37
3		2.0	11.9	2.48	14.20	0.48	1.74	13.20	15.70	17.30
D'	7	0.5	11.9	1.97	6.13	0.44	1.64	6.05	7.62	8.36
	8	2.0	11.9	1.97	9.88	0.38	1.54	9.88	12.48	13.59
	9	2.0	11.9	1.97	13.11	0.33	1.44	13.18	16.14	17.11
	10	2.0	15.8	2.02	9.62	0.38	1.61	9.74	12.48	14.00
	11	2.0	15.8	2.02	12.83	0.34	1.55	13.21	16.80	17.87
E'	12	0.5	11.9	1.53	5.05	0.38	1.29	5.05	6.72	7.75
	13	2.0	11.9	1.53	7.13	0.35	1.29	7.26	9.70	11.11
	14	2.0	11.9	1.53	9.93	0.31	1.23	10.19	13.38	14.90
	15	2.0	15.8	1.48	6.60	0.34	1.30	6.58	8.15	8.78
	16	2.0	15.8	1.48	9.41	0.32	1.26	9.53	12.03	13.34
F'	17	0.5	11.9	2.48	7.21	0.49	1.72	6.96	8.68	9.61
	18	2.0	11.9	2.48	11.68	0.42	1.56	11.51	14.39	15.63
	19	2.0	11.9	2.48	15.33	0.37	1.39	14.95	18.09	19.39
	20	2.0	15.8	2.59	6.43	0.47	1.80	6.18	7.78	8.58
	21	2.0	15.8	2.59	8.82	0.44	1.72	8.54	10.95	12.45
G'	22	0.5	11.9	1.97	7.62	0.42	1.50	7.53	9.53	10.62
	23	2.0	11.9	1.97	12.07	0.37	1.36	11.99	14.93	16.22
	24	2.0	11.9	1.97	15.42	0.35	1.30	15.21	17.95	18.99
	25	2.0	15.8	2.02	11.92	0.37	1.44	11.98	15.06	16.67
	26	2.0	15.8	2.02	15.34	0.35	1.34	15.36	18.64	20.03

variables could be reduced because the mean and standard deviation of the profile parameters were a function of the mean damage. The relation for the eroded depth was $\bar{E} = 0.44\bar{S}^{0.52}$ indicating that the shape of the eroded area remained geometrically similar during damage progression. Figure 4 shows \bar{E} for the four new series as a function of \bar{S} . The normalized eroded length followed $\bar{L} = 4.6\bar{S}^{0.48}$. This relation is shown in Figure 5. Finally, the mean cover depth was shown to be described by the relation $(\bar{C}_0 - \bar{C}) = 0.1\bar{S}$, where the subscript 0 indicates the initial value at $\bar{S} = 0$. This relation provides a very good fit, as shown in Figure 6.

These relationships for the damage variables as a function of mean damage (Figures 4-6) allow for prediction of profile shape and alongshore variability of damage.

Acknowledgements

This work was funded by the Coastal Structures Evaluation and Design Research Program, Headquarters, U.S. Army Corps of Engineers (HQUSACE). Permission was granted by the Office, Chief of Engineers, to publish this information. Mr. John Winkelman, U.S. Army Engineer District, San Francisco, is acknowledged for developing the automated breakwater profiler and

assisting with initial stages of the experiment.

References

Broderick, L. and Ahrens, J. P. (1982). "Rip-rap stability scale effects," Technical Paper 82-3, U.S. Army Engineer Waterways Experiment Station, Coastal Engineering Research Center, Vicksburg, MS.

Hudson, R. Y. (1959). "Laboratory investigation of rubble-mound breakwaters," *Journal of Waterways and Harbors Division*, American Society of Civil Engineers, 85 (WW3), 93-121.

Mansard, E. P. D., Davies, M. H., and Caron, O. (1996). "Model study of reservoir riprap stability." *Proceedings, 25th Coastal Engineering Conference*, 2, 1748-61.

Melby, J. A. and Kobayashi, N. (1998a). "Damage progression on rubble-mound breakwaters," Technical Report (in preparation). U.S. Army Engineer Waterways Experiment Station, Vicksburg, MS.

_____. (1998b). "Progression and variability of damage on

rubble-mound breakwaters," *Journal of Waterway, Port, Coastal, and Ocean Engineering*, American Society of Civil Engineers, 124 (6).

_____. (1998). "Damage progression on breakwaters." *Proceedings, 26th Conference on Coastal Engineering*, American Society of Civil Engineers, Copenhagen, Denmark, 2, 1,884-97.

Shore Protection Manual. (1984). 4th ed., 2 Vol., U.S. Army Engineer Waterways Experiment Station,

U.S. Government Printing Office, Washington, DC.

Van der Meer, J. (1988). *Rock slopes and gravel beaches under wave attack*. Delft Hydraulics Communication No. 396, Delft Hydraulics Laboratory, The Netherlands.

Winkleman, J. (1997). "Rubble mound damage measurement," M.S. thesis, University of Rhode Island, Kingston, RI.

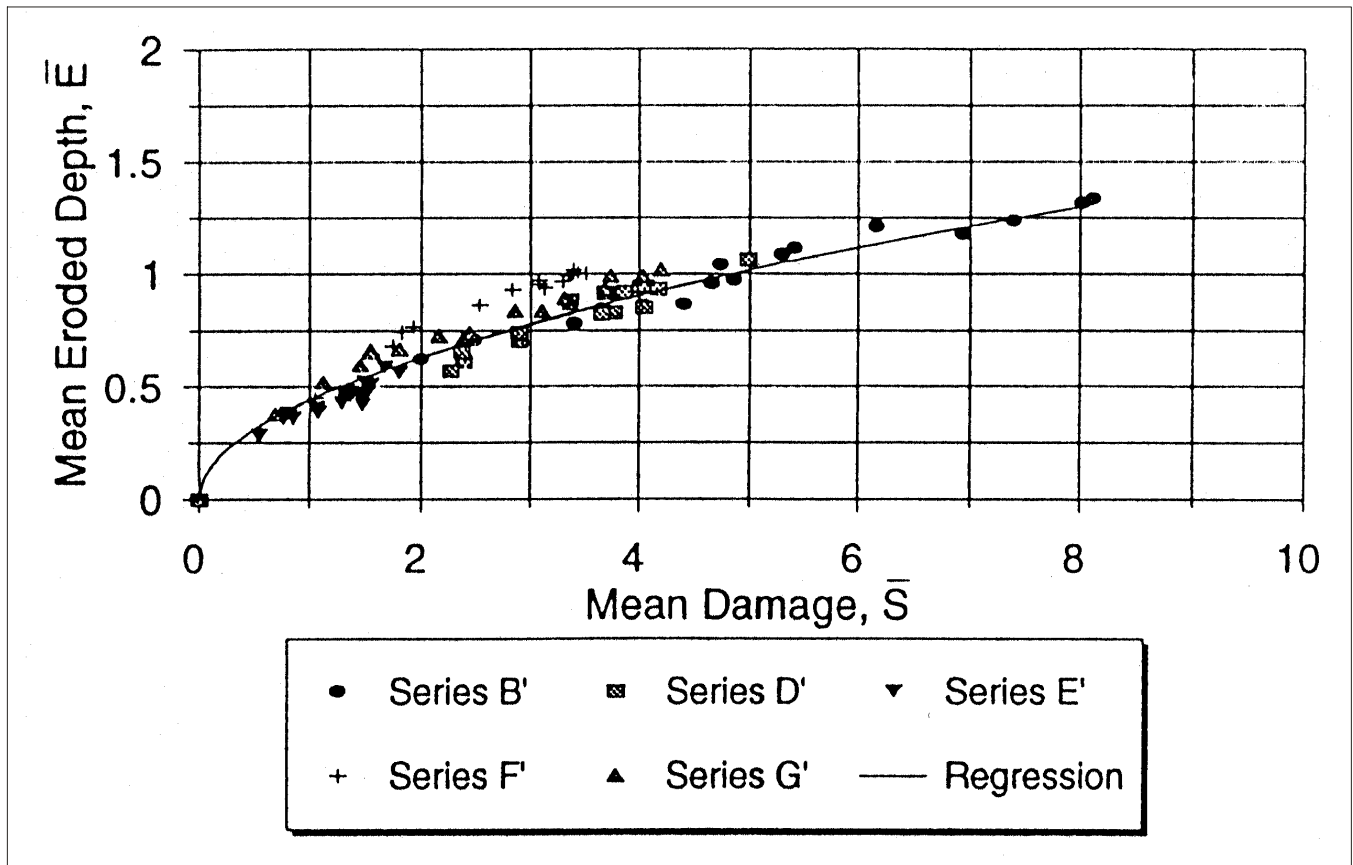


Figure 4. Mean normalized eroded depth as a function of mean damage

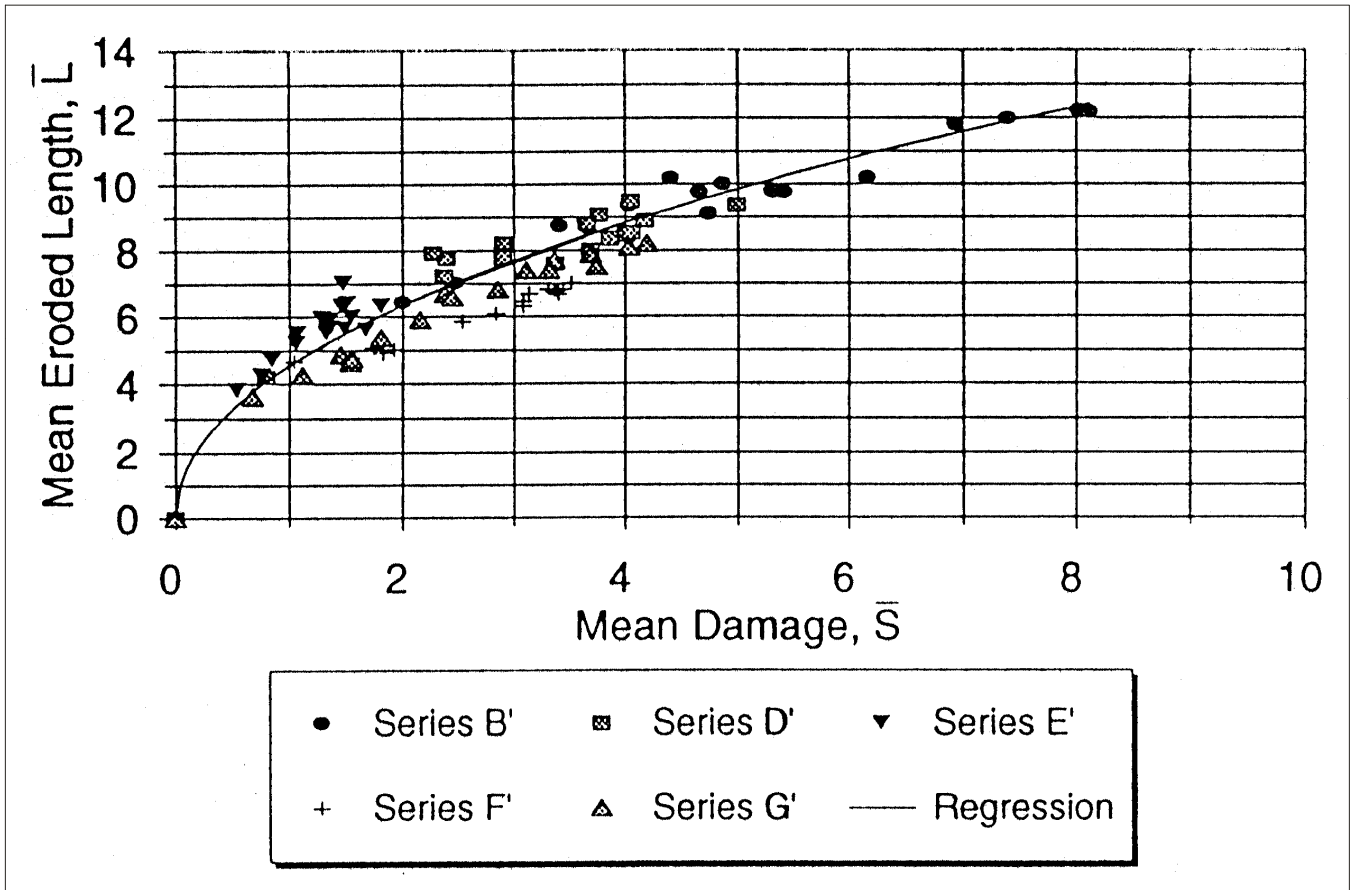


Figure 5. Mean normalized eroded length as a function of mean damage

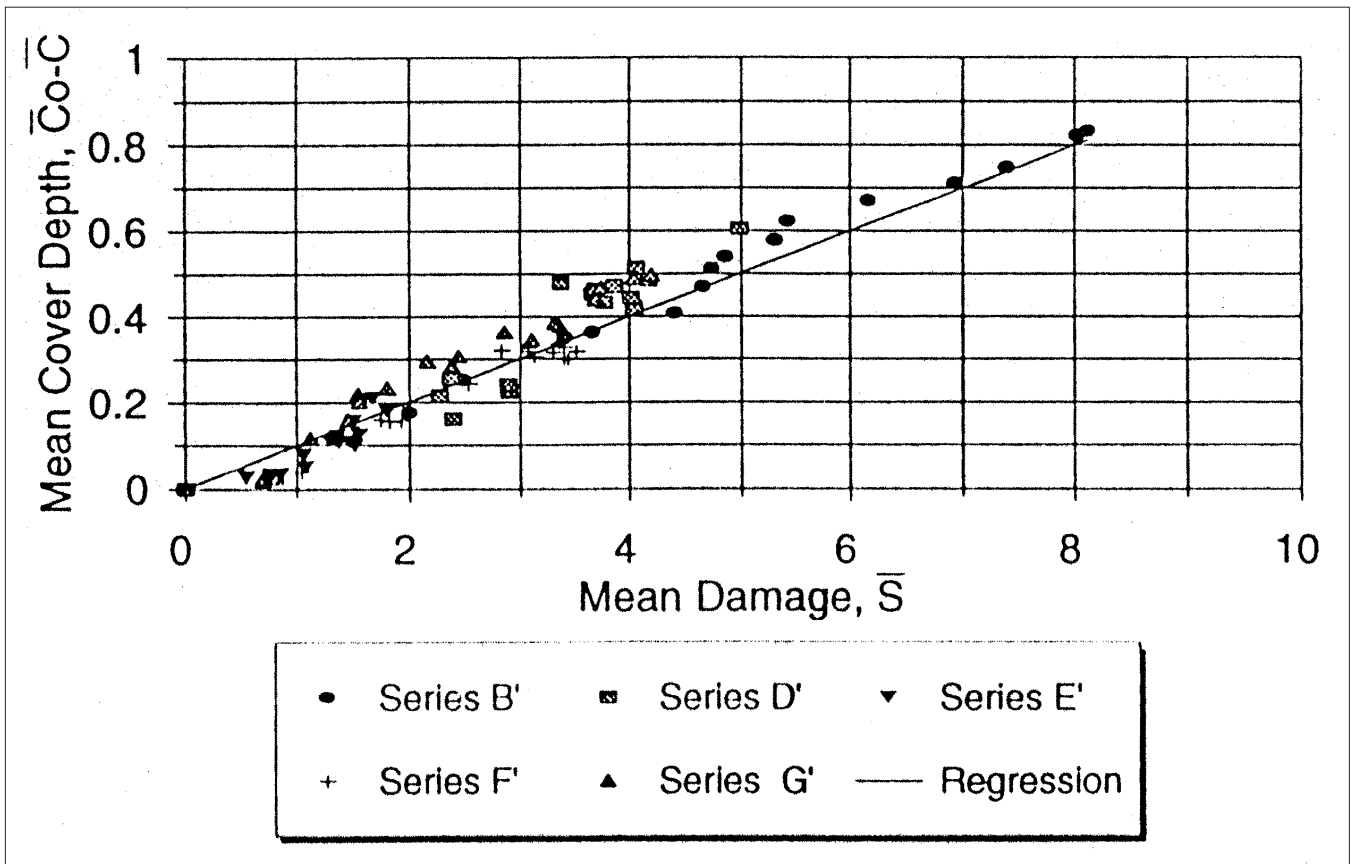


Figure 6. Mean normalized cover depth as a function of mean damage

Pressure and Acceleration Tests, Lock and Dam No. 1, Mississippi River near St. Paul, MN

Tim Fagerburg¹

Purpose of Study

Pressure and accelerations tests were conducted by the U.S. Army Engineer Research and Development Center during March 2000 to determine the effects of certain extreme flow regimes on the hydraulic performance of Lock and Dam No. 1 on the Mississippi River, located approximately 16.09 km (10 miles) south of St. Paul, MN. In emergency situations, this lock will be used as a flow release mechanism as the dam presently has an uncontrolled spillway (inflatable rubber dike). If, for example, an upstream bridge should fail, then the pool elevation would need to be significantly lowered very rapidly to expedite remedial operations. Such a rapid drawdown might induce unacceptable (even catastrophic) vibrations or pressures within the lock and dam structure.

Introduction

Pressure transducers and accelerometers were installed at the upper pool, lock chamber, and downstream pool locations. As each transducer was installed, cables were routed along the upper land wall to the recording area (Figures 1-3). The cables were connected to the data acquisition system (Figure 4). A triaxial accelerometer to monitor vibrations was mounted on the intermediate lock I-wall (Figure 5).

The sequence for the lock operations performed during the data collection is listed in Table 1. The following procedures for normal lock operations were followed for each



Figure 1. Upper pool water level pressure transducer location



Figure 2. Fill valve well water level pressure transducer

¹ Research Hydraulic Engineer, Tidal Hydraulics Branch, Coastal and Hydraulics Laboratory, U.S. Army Engineer Research and Development Center, Vicksburg, MS 39180

period of data recording to provide consistency in the data collection and to provide assurance that all instruments were zeroed to a known reference datum. Prior to any period of data collection, the miter gates (upper or lower, depending on the lock chamber water level) were opened slightly to equalize the water level in the lock chamber and dissipate any water surface oscillations resulting from the previous operation. When the lock was empty (the water surface at the lower pool elevation), all instrument readings were set at zero for the existing lower pool water level elevation. The data acquisition system was activated to begin recording data for 30 sec to collect baseline information on all instruments. The miter gates were closed and the operation of the filling or emptying valves was initiated. Once the lock was empty or full, the miter gates were then opened slightly to equalize the water level in the lock chamber and to dissipate any water surface oscillations. When the lock chamber water surface appeared to be calm, data recording was stopped.

Normal Lock Operations

Normal lock operations for filling and emptying cycles were monitored to observe the pressures, valve movements, and I-wall vibrations for the currently programmed valve movements and incremental valve movements. The current programmed lock operation for a filling cycle is for the fill valve to stop at 25 percent open for approximately 15 sec, continue opening, stop again at 50 percent open for approximately 60 sec, and then continue opening to 100 percent (Figure 6). The observed time for the valve operation is 157 sec. During the empty cycle of the programmed lock operation, the opening of the empty valve is continuous from the closed position to the full open position. The empty valve opening operation time was observed to be 83 sec. The incremental valve opening (as recommended by a previous model study) consists of opening the fill valve in 25 percent increments and holding for approximately 60 sec

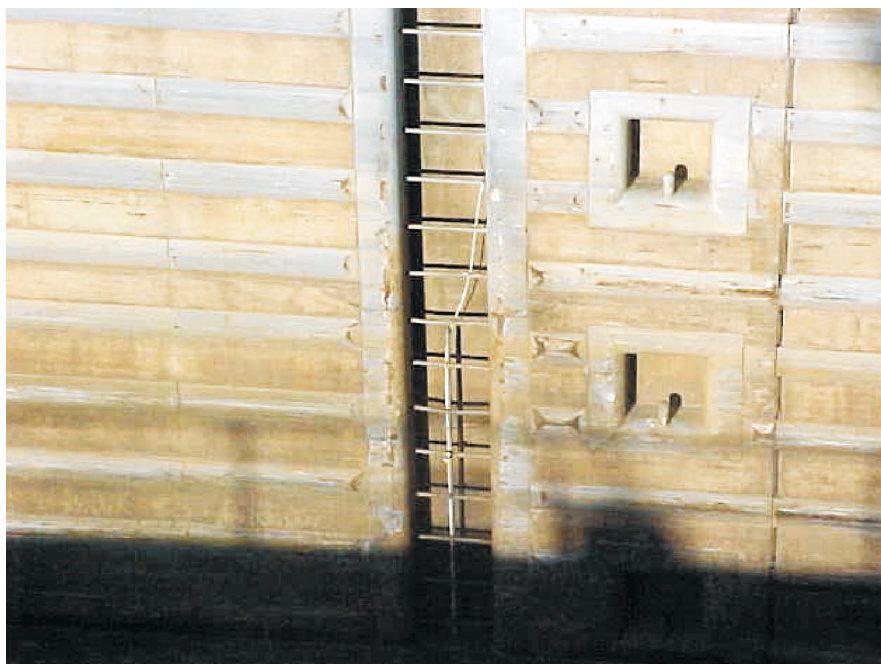


Figure 3. Lower pool pressure transducer location in the ladder well recess on the land wall



Figure 4. Checking instruments at the data acquisition system location

before proceeding to the next opening, thus requiring a total of 4 min to reach the full open position (Figure 7). During a normal lock filling operation, the culvert soffit pressures immediately downstream of the fill valve were observed to be lowest at valve openings of 50 percent (Figure 8). The greatest drawdown of the

water level in the fill valve well was observed to occur at 100 percent valve openings (Figure 9).

Operations of the fill and empty valves were performed to determine the effect of closing the valves during the period of lowest pressures at the culvert soffit. During these operations, the valves were

operated normally, except that immediately before the valves began to open from the 50 percent increment, closing procedures were initiated to simulate emergency valve closure operations. The data recorded by the inclinometers indicated no potential problem with valve closure under these circumstances.

Non-Normal Lock Operations

Non-normal lock operations refer to conditions under which the lock structure might be utilized to provide additional discharge capacity during emergency pool drawdown procedures (Figures 10 and 11). These types of lock operations were conducted to determine the hydraulic conditions that result from the various configurations of fill valves, empty valves, and miter gates.

The first of a series of flow releases using the lock structure culvert system was performed using the same operating procedures that had been used in previous operations for flow releases. Initially a split head differential was established between the upper pool and the water level in the lock chamber at half-full (709.23 ft).¹ The fill valves and empty valves were opened to the full open position. The empty valve opening lagged 3 sec behind the fill valve opening. During the initial part of the flow release operation, the fill valve remained in the full open position and the water level in the lock chamber was controlled using the empty valve. During the latter part of the operation, adjustments to both of the valves were continuously made to maintain the water surface in the lock chamber at the half-full level. Figure 12 depicts the time-history of this operation. The lowest pressure downstream of the empty valve was -11.6 ft (el 674.6) below the culvert soffit. The lowest pressure recorded



Figure 5. Triaxial accelerometer mounted on the I-wall

Table 1. Lock Operation Schedule for Field Data Collection

Lock Operation Description	Fill	Empty
1. Normal Lock Fill and Empty Operation Procedures		
a. 4 min valve opening time (model study recommendation)	X	X
b. Actual operation (modified valve schedule) 10-12 min fill time	X	X
c. Same as a using only landside valves	X	X
d. Same as b using only landside valves	X	X
2. Non-Normal Lock Operations		
a. Split head differential by partially filling lock (Lock ½ full)		
(1) 100% valve opening		X
(2) 60% valve opening		X
(3) 40% valve opening		X
(4) 20% valve opening		X
b. Passing of flow with lock empty and lower miter gates open		
(1) 40% valve opening		X
(2) 20% valve opening		X
Total Number of Tests		14

downstream of the fill valve was 4.6 ft (el 690.8) above the culvert soffit. These low pressures were instantaneous responses to changes in the valve openings.

A second operation for flow release using the lock chamber was performed. For this operation, the lower miter gates were locked in the open position, the lock chamber water surface was at the lower pool

elevation, the empty valves were closed, and then the fill gates were opened in increments. The first open was set to 20 percent for approximately 7.5 min. The fill valve was then opened to 40 percent for the remainder of the operation (Figure 13). Fill valve openings above 40 percent were prohibited for safety reasons. A requirement to perform this type of operation is that the

1 All elevations (el) cited herein are in feet referenced to the National Geodetic Vertical Datum (NGVD). (To convert feet to meters, multiply by 0.3048).

lower miter gates be locked in the open position by pinning them to the wall in the miter gate recesses. As a precautionary measure, this procedure is followed to prevent the gates from closing as a result of any significant flow forces in the lock chamber and gate recess areas. The flow patterns and resulting forces that could be generated from this type of operation could be significant enough to overpower the gates' hydraulic operating system. If this were to occur, severe damage to the miter gates would result from the uncontrolled closing. The lowest pressures recorded at the culvert soffit below the fill valve were -12.3 ft (el 673.9) below the culvert soffit, and occurred when the valve went past the 40 percent valve open position. No significant pressure fluctuations were recorded during this operation. The average pressure at the 40 percent valve opening was -10.6 ft (el 675.6) below the culvert soffit.

A third flow release operation was performed similar to that described in the first series above, with the following changes. Initially, the lock chamber was full (pool el 726.6), the fill valve was set at the full open 100 percent position, and the empty valve was opened in 10 percent increments. Each incremental opening of the empty valve was held at that position for an average of 120 sec. Figure 14 presents the time-histories of the culvert pressures, lock chamber water surface elevations, and the empty valve openings for this flow release operation. Culvert soffit pressures below the fill valve followed closely and slightly lower than the lock chamber water surface elevations. The lowest average pressure recorded below the fill valve was 13.0 ft above the culvert soffit (el 699.2). No static pressure conditions were reached at this location due to the continual lowering of the lock chamber water surface. The culvert soffit pressures below the empty valve changed with each increment of valve opening. The lowest average pressure below the empty valve was -10.0 ft below the culvert soffit (el 676.2) and occurred at the valve opening of 70 percent. No significant fluctuations were evident in the recorded data.

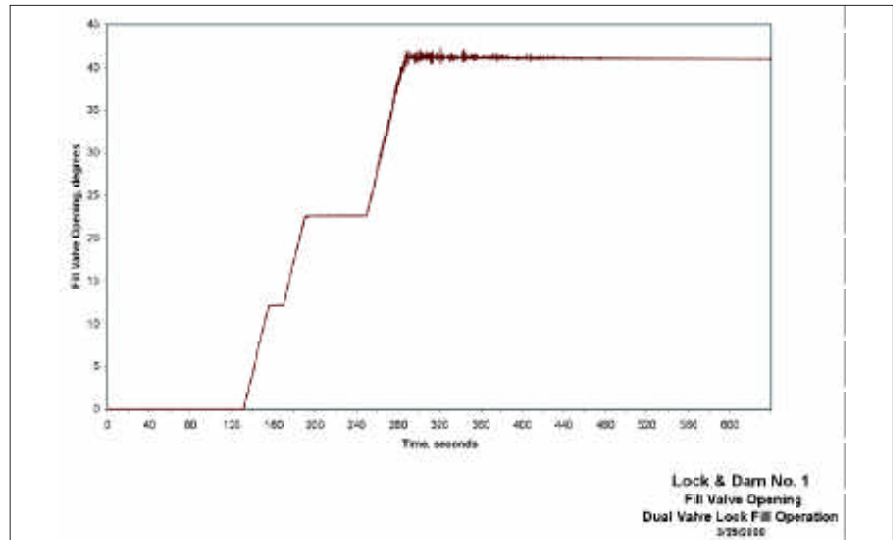


Figure 6. Time-history of sequential fill valve opening

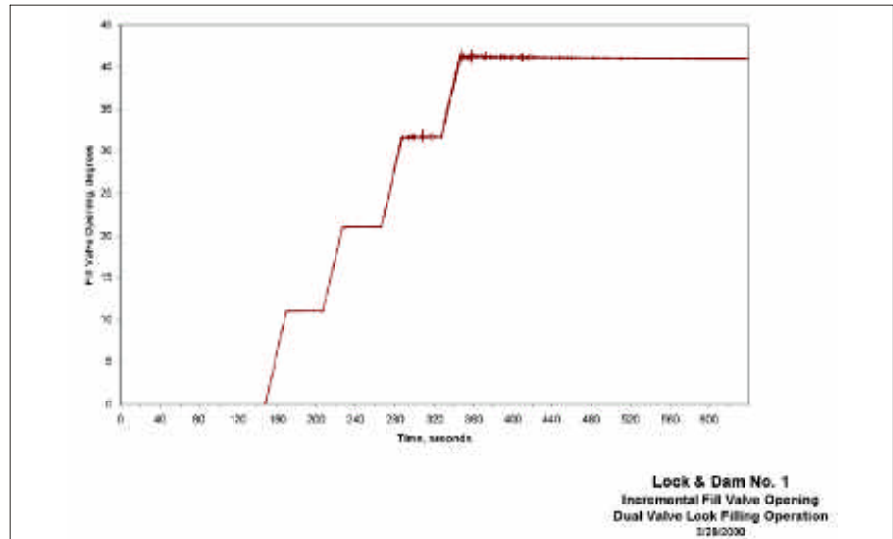


Figure 7. Time-history of incremental fill valve opening during a normal lock filling operation

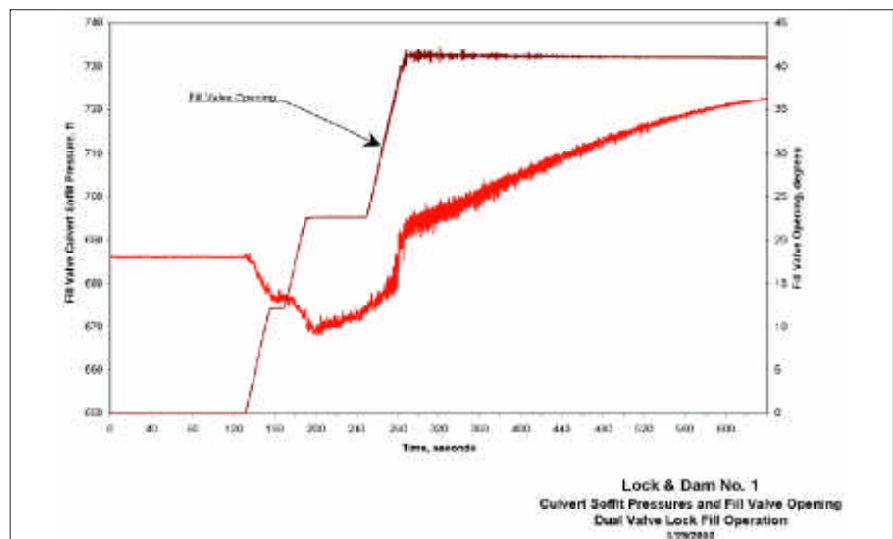


Figure 8. Time-history of fill valve culvert soffit pressures and fill valve opening during a normal lock filling operation (to convert feet to meters, multiply by 0.3048)

A fourth series of lock operations were then performed using only the land wall culvert valves for the filling and emptying of the lock chamber. The valves were operated under two different conditions; (a) valve openings with no programmed stops during the opening, and (b) openings of 25 percent increments over a 4-min time period. The results of lock operations with valves opened completely with no programmed stops are shown in Figures 15 and 16. During the lock empty test, the lowest empty valve culvert soffit pressure was -8.2 ft (el 678.0) below the culvert soffit and occurred at a valve opening of 50 percent. The lowest fill valve culvert soffit pressure during the lock filling operation was -14.3 ft (el 671.9) below the culvert soffit. The results of single valve lock operations, filling and emptying, with the valves opened in 25 percent increments are shown in Figures 17 and 18. The lowest recorded culvert soffit pressures for the empty and fill operations were -9.0 ft (el 677.2) and -10.6 ft (el 675.6), respectively.

Valve Movement

In all the lock operations where the fill valve was at the 100 percent open position, there appeared to be significant movement of the valve [3.3 deg or 0.1524 m (0.5 ft)] due to the high velocities and the low head in the lock chamber (Figure 19). This condition would persist for a period of time (60 to 80 sec) until sufficient water levels in the fill valve well and lock chamber (el 712.0) were reached and the velocities at the valve decreased. Visual observations of the lift cable movement were noted during these periods of valve movement (approximately 3 to 4 in. back and forth). This condition may be the result of the valve lifting eye protruding into the flow below the elevation of the culvert soffit, and had been previously noted. Vibrations of the empty valve lifting cable also were observed during the lock emptying operations, although these conditions were not as extreme as those for the fill valve. Any long-term operation of the valves under these conditions should be avoided. Consideration

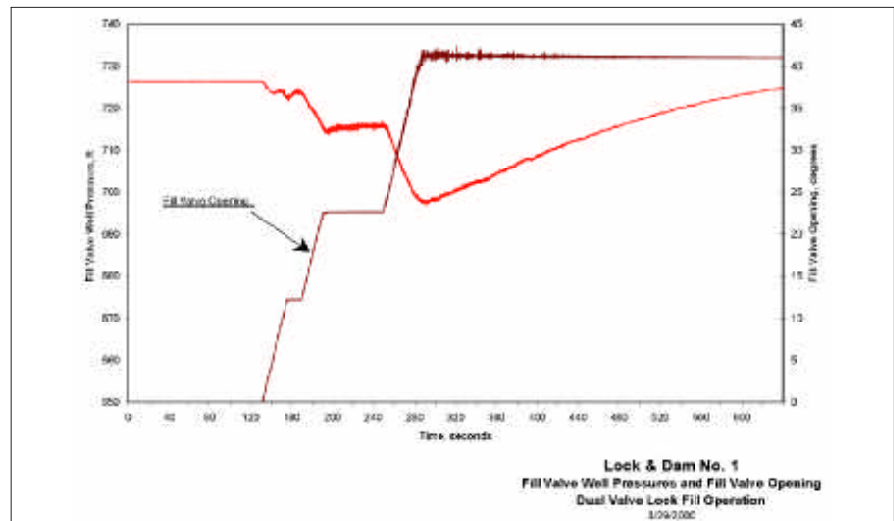


Figure 9. Time-history of fill valve well pressures and fill valve opening during a normal lock filling operation

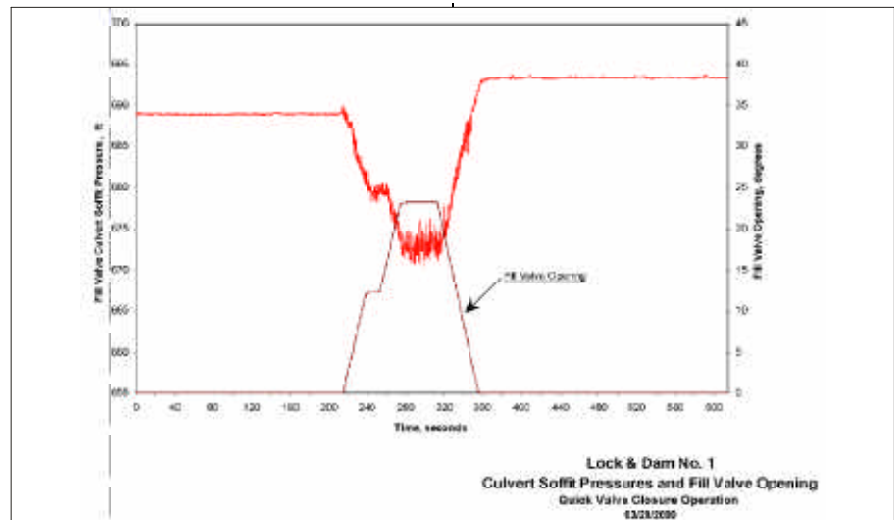


Figure 10. Time-history of fill valve opening and closing to simulate emergency valve closing during a lock filling operation

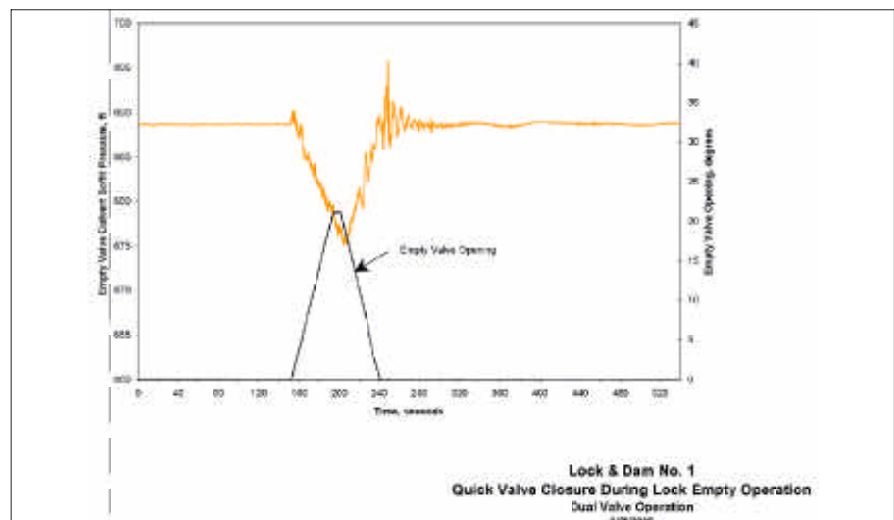


Figure 11. Time-history of empty valve opening and closing to simulate emergency valve closing during a lock emptying operation

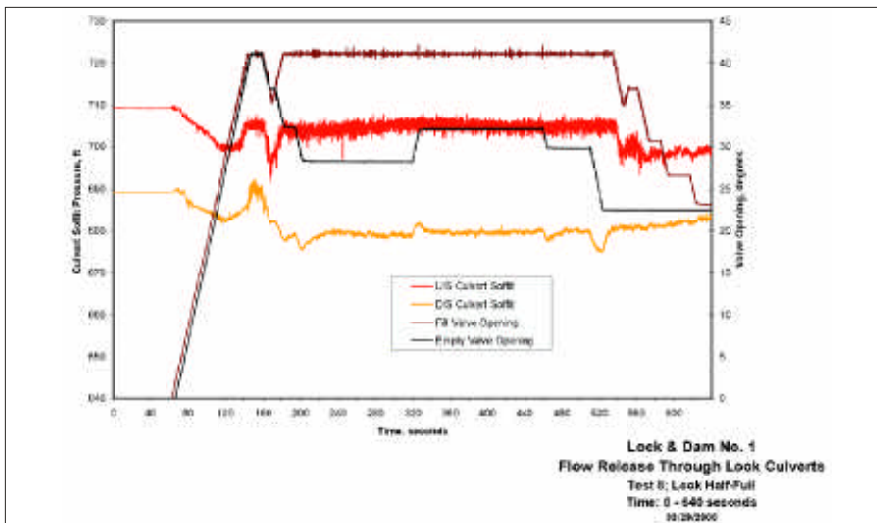


Figure 12. Time-history of culvert soffit pressures and valve openings for flow releases through the lock culverts (Continued)

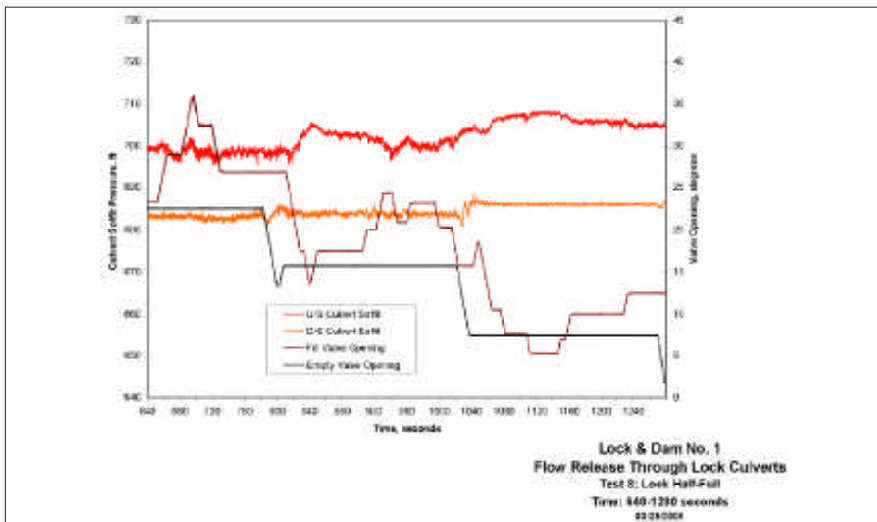


Figure 12. (Concluded)

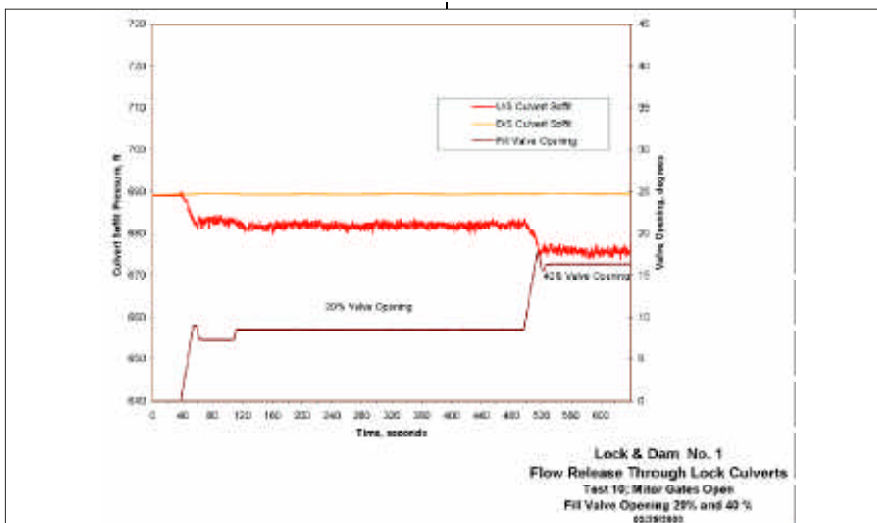


Figure 13. Time-history of culvert soffit pressures and valve opening for flow releases through lock culverts with the lower miter gates open

should be given to determine if modifications can be made to increase the limit settings for the valve openings to raise the valve lifting beam above the elevation of the culvert soffit.

I-Wall Vibrations

As part of the overall data collection program, vibrations of the I-wall were monitored during all lock operations. The inclusion of vibration monitoring in the data collection resulted from observations made by the U.S. Army Engineer District, St. Paul, personnel during previous lock operations. These observations were made during a period when the land lock chamber filling system was used to release water for an emergency drawdown of the upper pool. It was during this event that personnel detected significant vibrations of the I-wall. During this subject data collection effort, the flow conditions from the previous operation could not be duplicated.

Conclusions

No significant vibration levels were detected during the normal lock operations. Vibration levels were very low, ranging from 0.000 g during the majority of the operation to 0.012 g during non-normal lock operations. The acoustics from the air being drawn into the bulkhead slots and the valve wells were the most severe conditions observed during the various operations. This condition was especially evident during the single valve lock fill operation. The air drawn into the culvert intake bulkhead slots caused the steel cover plat to deflect approximately one-half to three-quarters of an inch. The noise level created by this operation was significantly higher and more disturbing than the structural vibration levels.

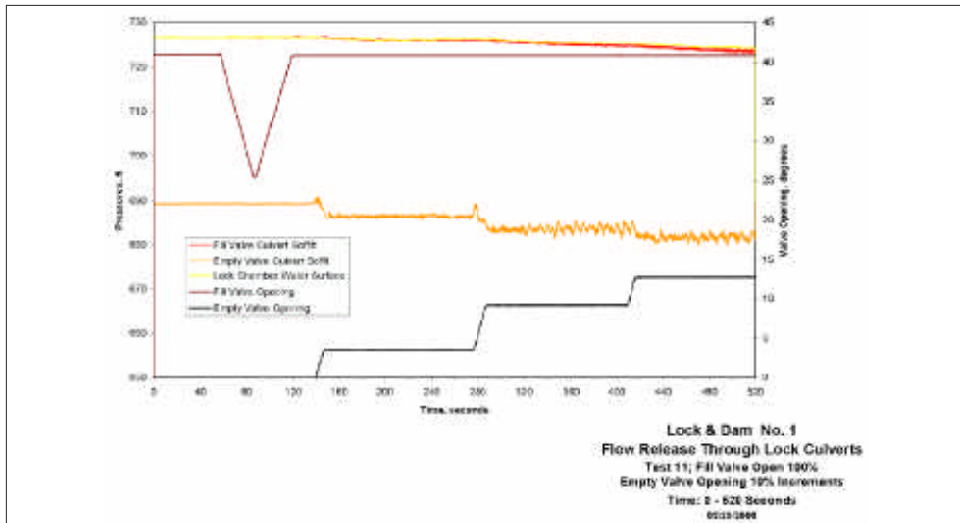


Figure 14. Time-history of culvert pressures, lock chamber water surface, and valve opening for flow release operation (Continued)

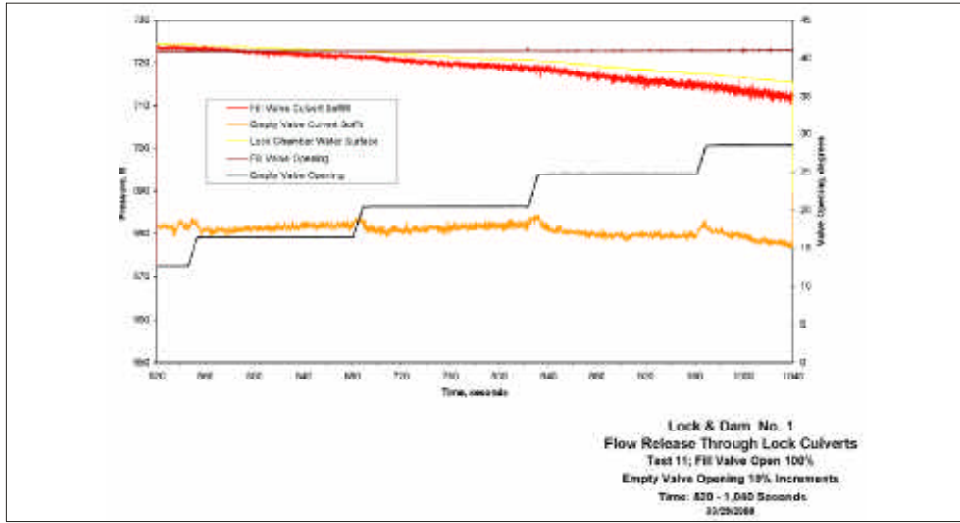


Figure 14. (Continued)

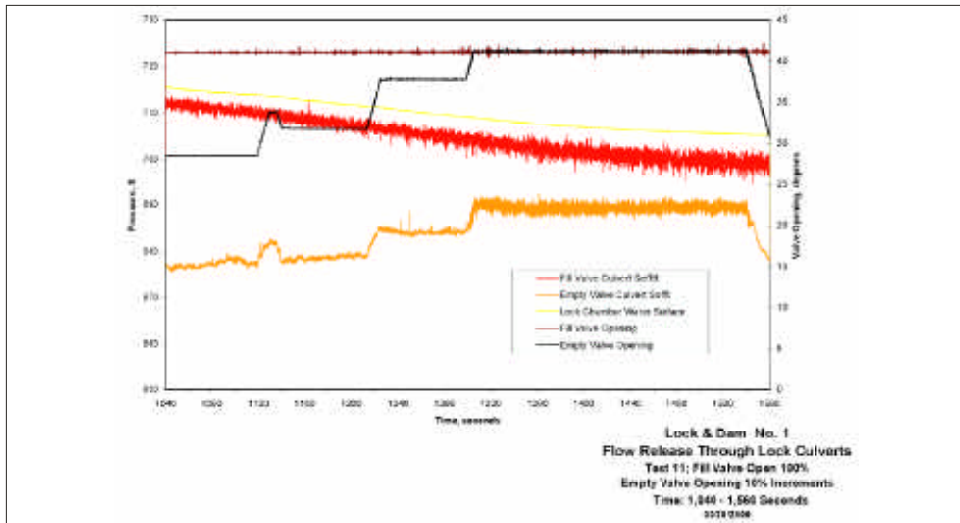


Figure 14. (Concluded)

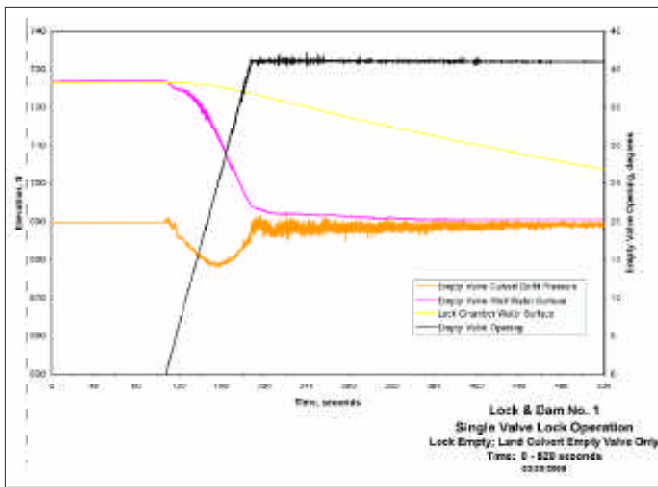


Figure 15. Time-history of culvert pressure, lock chamber water surface, empty valve well water surface, and empty valve opening for a single valve lock emptying operation (Continued)

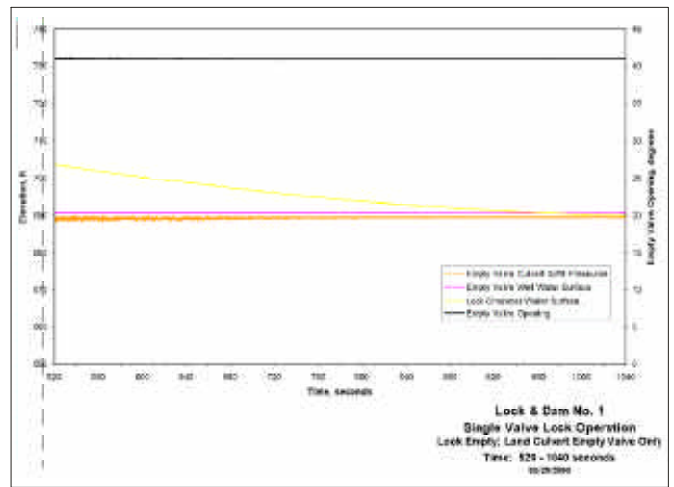


Figure 15. (Concluded)

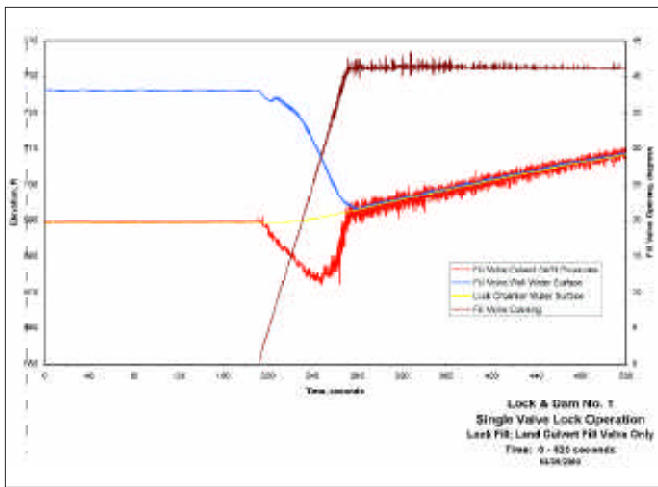


Figure 16. Time-history of culvert pressures, fill valve well water surface, lock chamber water surface and fill valve opening for a single valve lock filling operation (Continued)

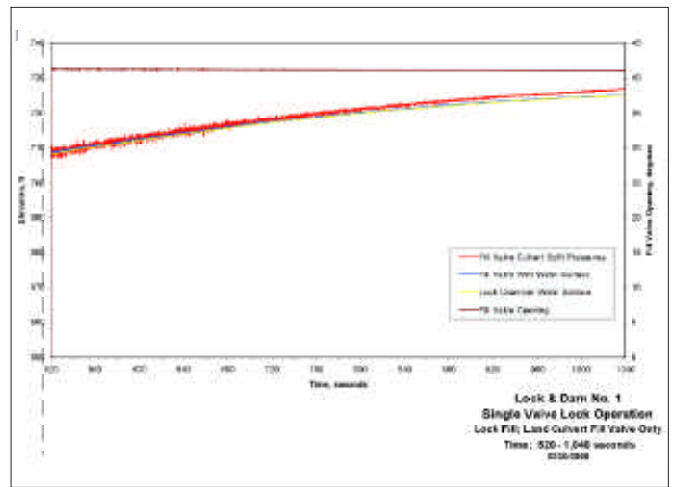


Figure 16. (Concluded)

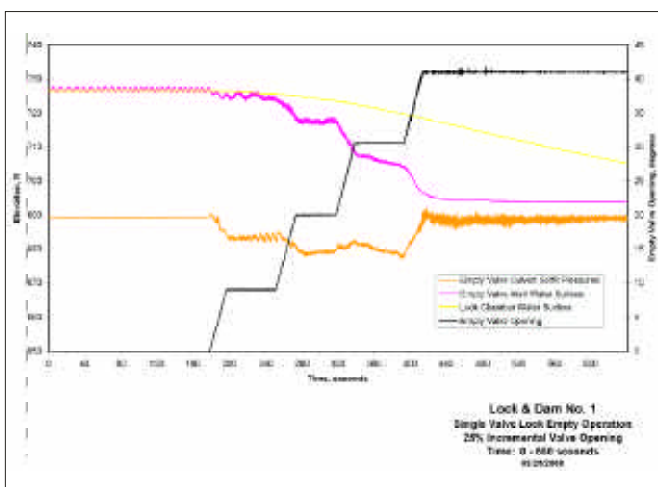


Figure 17. Time-history of culvert pressure, empty valve well water surface, lock chamber water surface and empty valve openings for a single valve lock empty operation with incremental valve opening (Continued)

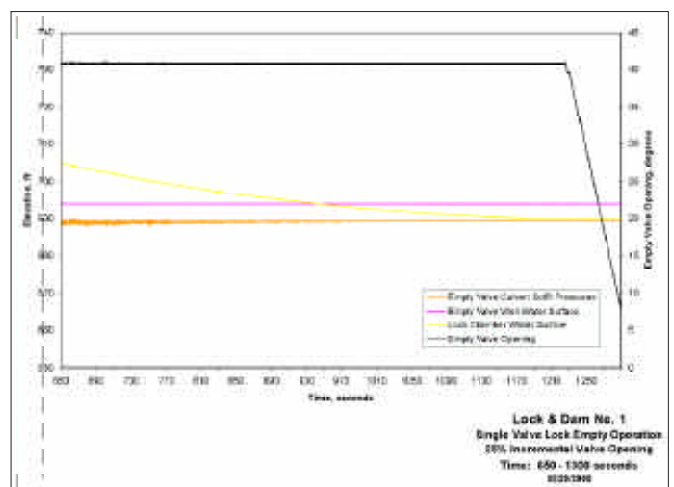


Figure 17. (Concluded)

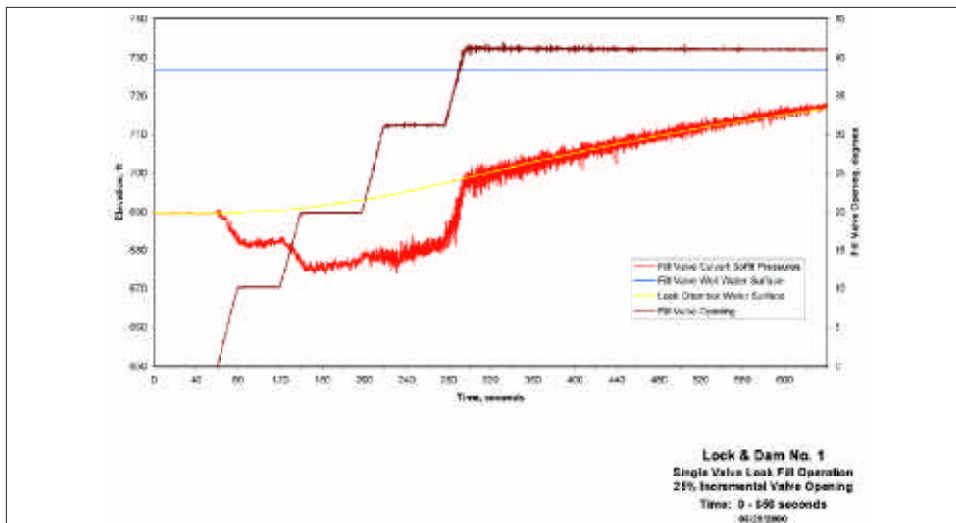


Figure 18. Time-history of culvert pressure, fill valve well water surface, lock chamber water surface and fill valve opening for a single valve lock filling operation with incremental valve opening (Continued)

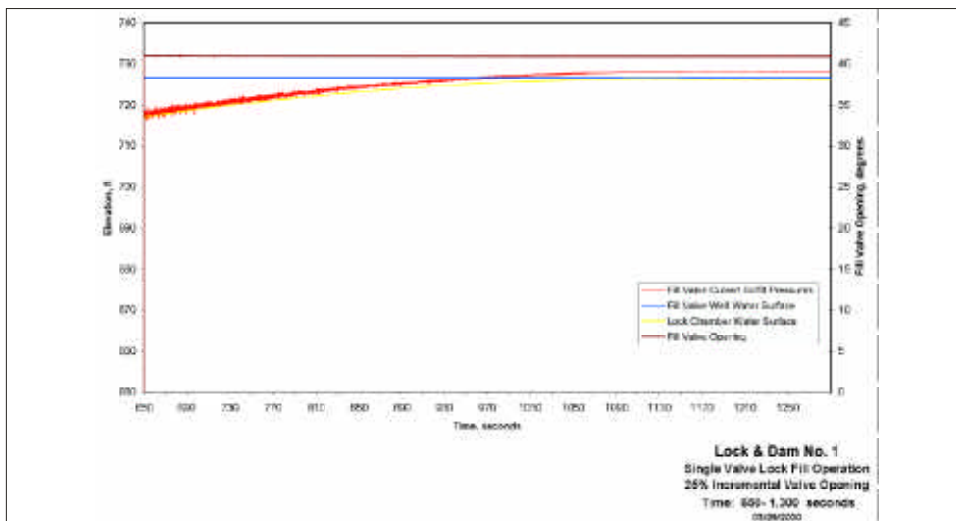


Figure 18. (Concluded)

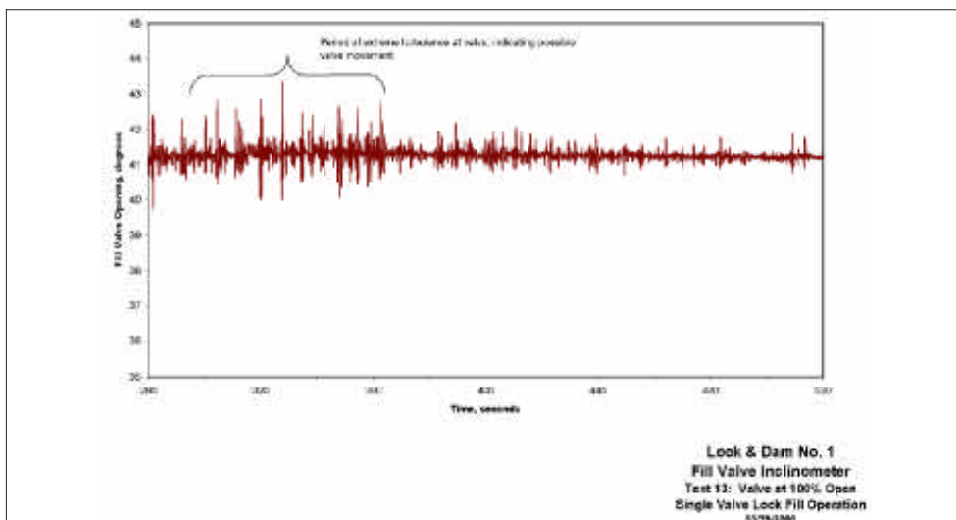


Figure 19. Time-history of fill valve inclinometer indicating possible valve movement during periods of extreme turbulence in the valve well area



**US Army Corps
of Engineers**
Engineer Research and
Development Center

Coastal and Hydraulics News

Coastal and Hydraulics Laboratory
U.S. Army Engineer Research and Development Center
Vicksburg, Mississippi 39180-6199

This bulletin is prepared in accordance with AR 25-30 as an information dissemination function of the U.S. Army Engineer Research and Development Center (ERDC). The publication is part of the technology transfer mission of the Coastal and Hydraulics Laboratory (CHL) of ERDC under PL 79-166 and PL 99-802. Results from ongoing research programs will be presented. Special emphasis will be placed on articles relating to application of research results or technology to specific project needs.

Contributions of pertinent information are solicited from all sources and will be considered for publication. Communications are welcomed and should be addressed to the U.S. Army Engineer Research and Development Center, Coastal and Hydraulics Laboratory, ATTN: Dr. Lyndell Z. Hales, 3909 Halls Ferry Road, Vicksburg, MS 39180-6199, or call (601) 634-3207, FAX (601) 634-4253, Internet: Lyndell.Z.Hales@erdc.usace.army.mil


JAMES R. HOUSTON, PhD
Director